Cell Stem Cell

Article

# Disrupting Mitochondrial Copper Distribution Inhibits Leukemic Stem Cell Self-Renewal

## Graphical Abstract

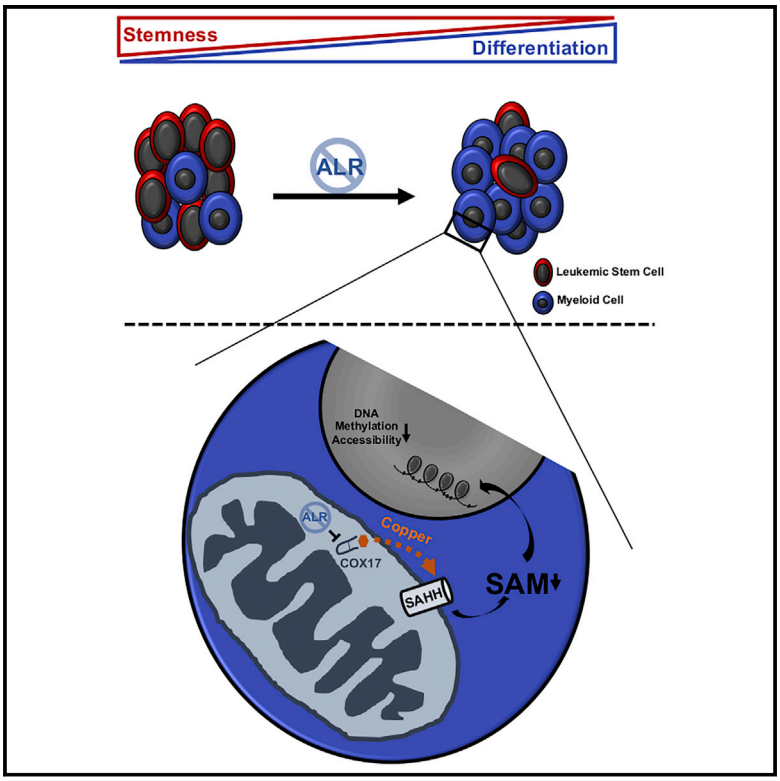


## Highlights

- The sulfhydryl oxidase ALR is necessary for the viability of AML cells and LSCs
- Loss of MIA/ALR substrate COX17 redistributes mitochondrial copper
- Redistribution of mitochondrial copper reduces DNA methylation and accessibility
- Copper-regulated epigenetic changes result in LSC differentiation

## Authors

Rashim Pal Singh, Danny V. Jeyaraju, Veronique Voisin, ..., Gary D. Bader, Mathieu Lupien, Aaron D. Schimmer

## Correspondence

aaron.schimmer@uhn.ca

## In Brief

Singh et al. demonstrate that modulating the mitochondrial intermembrane assembly (MIA) pathway leads to decreased viability of AML cells. Targeting the sulfhydryl oxidase ALR results in loss of copper chaperone COX17 and redistribution of mitochondrial copper, causing decreased DNA methylation, chromatin accessibility, and self-renewal of leukemic stem cells (LSCs).

Singh et al., 2020, Cell Stem Cell *26*, 1–12
June 4, 2020 
https://doi.org/10.1016/j.stem.2020.04.010

CellPress

Cell Stem Cell

CellPress

Article

# Disrupting Mitochondrial Copper Distribution Inhibits Leukemic Stem Cell Self-Renewal

Rashim Pal Singh,[1,3] Danny V. Jeyaraju,[1,3] Veronique Voisin,[2] Rose Hurren,[1] Changjiang Xu,[2] James R. Hawley,[1] Samir H. Barghout,[1] Dilshad H. Khan,[1] Marcela Gronda,[1] Xiaoming Wang,[1] Yulia Jitkova,[1] David Sharon,[1] Sanduni Liyanagae,[1] Neil MacLean,[1] Ayesh K. Seneviratene,[1] Sara Mirali,[1] Adina Borenstein,[1] Geethu E. Thomas,[1] Joelle Soriano,[1] Elias Orouji,[1] Mark D. Minden,[1] Andrea Arruda,[1] Steven M. Chan,[1] Gary D. Bader,[2] Mathieu Lupien,[1] and Aaron D. Schimmer[1,4,*]

[1]Princess Margaret Cancer Centre, University Health Network, Toronto, ON, Canada
[2]The Donnelly Centre, University of Toronto, Toronto, ON, Canada
[3]These authors contributed equally
[4]Lead Contact
*Correspondence: aaron.schimmer@uhn.ca
https://doi.org/10.1016/j.stem.2020.04.010

## SUMMARY

Leukemic stem cells (LSCs) rely on oxidative metabolism and are differentially sensitive to targeting mitochondrial pathways, which spares normal hematopoietic cells. A subset of mitochondrial proteins is folded in the intermembrane space via the mitochondrial intermembrane assembly (MIA) pathway. We found increased mRNA expression of MIA pathway substrates in acute myeloid leukemia (AML) stem cells. Therefore, we evaluated the effects of inhibiting this pathway in AML. Genetic and chemical inhibition of ALR reduces AML growth and viability, disrupts LSC self-renewal, and induces their differentiation. ALR inhibition preferentially decreases its substrate COX17, a mitochondrial copper chaperone, and knockdown of COX17 phenocopies ALR loss. Inhibiting ALR and COX17 increases mitochondrial copper levels which in turn inhibit S-adenosylhomocysteine hydrolase (SAHH) and lower levels of S-adenosylmethionine (SAM), DNA methylation, and chromatin accessibility to lower LSC viability. These results provide insight into mechanisms through which mitochondrial copper controls epigenetic status and viability of LSCs.

## INTRODUCTION

Mitochondria regulate cell metabolism and produce ATP through oxidative phosphorylation. We and others have shown that AML cells and stem cells have unique mitochondrial characteristics with an increasing reliance on oxidative phosphorylation (Lagadinou et al., 2013; Skrtić et al., 2011; Sriskanthadevan et al., 2015). As such, targeting mitochondrial pathways such as mitochondrial protein synthesis and mitochondrial protein degradation preferentially kills AML cells over normal hematopoietic cells. For example, the mitochondrial protease ClpP is overexpressed in 45% of AML patients. This protease degrades damaged and misfolded respiratory chain complex proteins and thereby maintains the integrity of the respiratory chain. Inhibiting ClpP leads to impaired respiratory chain function and decreased oxidative phosphorylation and preferentially kills AML cells and stem cells *in vitro* and *in vivo* (Cole et al., 2015).

Mitochondria counterbalance the degradation of damaged or misfolded proteins by importing new proteins. Of the approximately 1,300 mitochondrial proteins, all but 13 are encoded by nuclear DNA, translated in the cytoplasm and imported into the mitochondria (Wiedemann and Pfanner, 2017). Precursor proteins synthesized in the cytosol traverse the outer mitochondrial membrane through the TOM (translocase of the outer membrane) complex. Once imported, mitochondrial proteins are routed to the membranes, intermembrane space (IMS) or matrix on the basis of their localizing sequences and interaction with translocases such as TIM23 and TIM22 (Wiedemann and Pfanner, 2017). A subset of cysteine-rich proteins destined for the mitochondrial IMS are oxidized and folded by the mitochondrial IMS assembly (MIA) pathway (Chacinska et al., 2004; Stojanovski et al., 2008). Key molecules of the MIA pathway are MIA40 and ALR (augmenter of liver regeneration) (Mordas and Tokatlidis, 2015). ALR is a flavin adenine dinucleotide (FAD)-linked sulfhydryl oxidase that acts in concert with MIA40 and uses oxygen and cytochrome *c* as final acceptor of electrons (Nalesnik et al., 2017) .

In the present study, we explored the effects of inhibiting folding of newly imported proteins in the mitochondrial IMS. Specifically, we focused on targeting ALR in AML and evaluated the role of ALR on AML stem cells and differentiation. Using chemical and genetic approaches, we demonstrated that ALR is necessary to maintain AML stem cell function. Inhibiting ALR led to reductions in its substrate, COX17. COX17 is a copper metal chaperone, and inhibiting ALR or COX17 increased mitochondrial copper. By controlling levels of mitochondrial copper, ALR and COX17 regulate levels of S-adenosylmethionine (SAM), DNA methylation, gene expression, and chromatin accessibility,

Please cite this article in press as: Singh et al., Disrupting Mitochondrial Copper Distribution Inhibits Leukemic Stem Cell Self-Renewal, Cell Stem Cell (2020), https://doi.org/10.1016/j.stem.2020.04.010



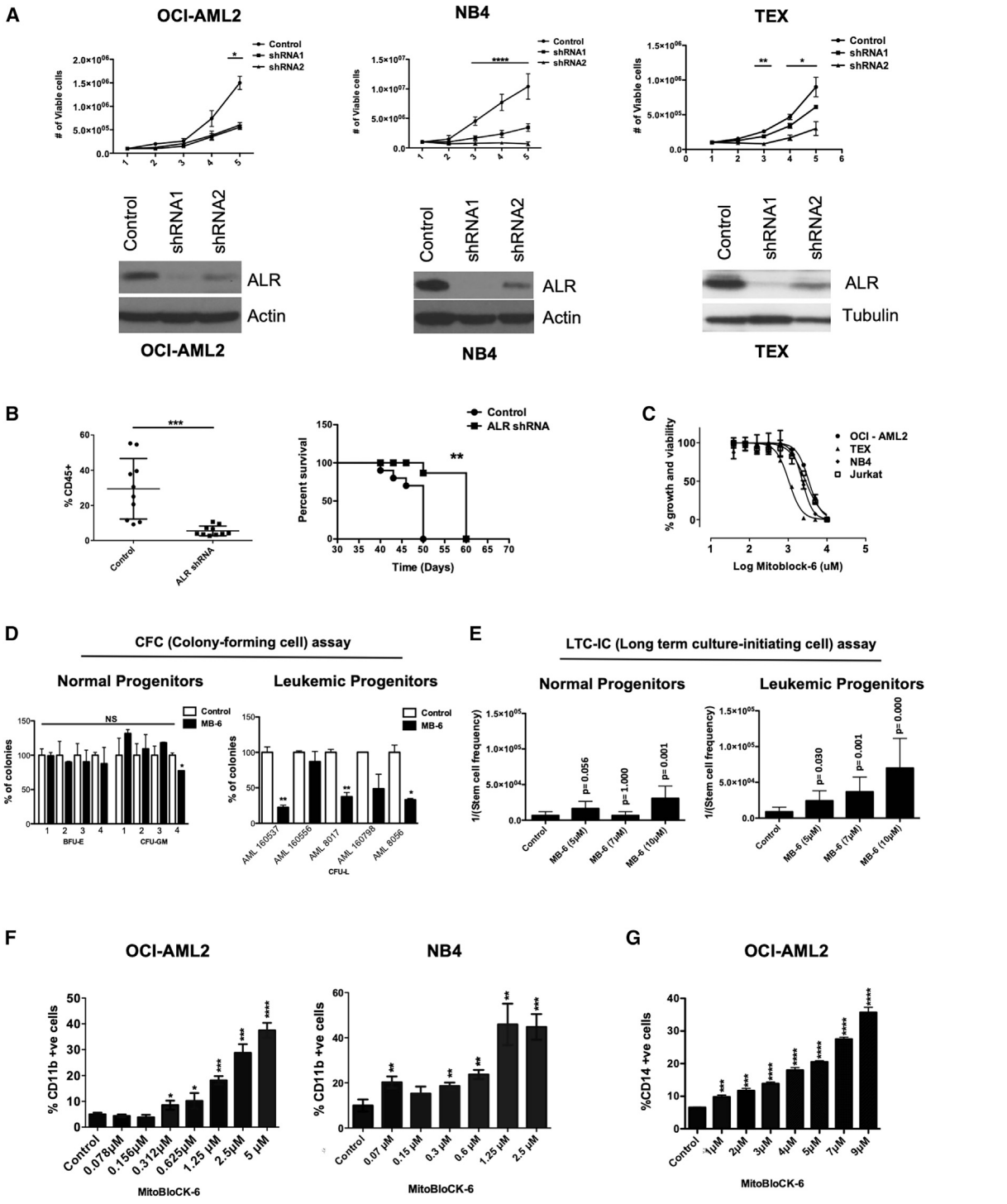


**Figure 1. Genetic and Chemical Inhibition of ALR Reduces Viability and Induces Differentiation of AML Cells**

(A) OCI-AML2, NB4, and TEX AML cells were transduced with shRNA targeting ALR or control sequences. Five days after transduction, levels of ALR were measured by immunoblotting. Growth and viability of the cells were measured by trypan blue exclusion staining.

(B) TEX cells transduced with shRNA targeting ALR or control sequences were injected into the right femur of sub-lethally irradiated NOD/SCID-GF mice. Five weeks post-injection, engraftment of TEX cells into the left femur was measured by flow cytometry. Survival was measured over time.

(C) Cell growth and viability of AML cells treated with increasing concentrations of MitoBloCK-6 as measured by MTS assay.

(D) Effects of MitoBloCK-6 (2 μM) on the clonogenic growth of primary AML (n = 5) and normal hemopoietic (n = 4) cells.

(E) Effects of MitoBloCK-6 on primary AML and normal hematopoietic cells as measured by the long-term culture and limiting dilution assay.

*(legend continued on next page)*

Please cite this article in press as: Singh et al., Disrupting Mitochondrial Copper Distribution Inhibits Leukemic Stem Cell Self-Renewal, Cell Stem Cell (2020), https://doi.org/10.1016/j.stem.2020.04.010





thereby affecting the viability of AML cells and stem cells. Thus, we describe a mechanism by which mitochondria regulate epigenetics, gene expression, and differentiation of malignant cells.

## RESULTS

### Genetic and Chemical Inhibition of ALR Reduces Viability and Induces Differentiation of AML Cells

We began our investigation of the MIA pathway by studying the expression of MIA40/ALR substrates in leukemic stem cell (LSC+) versus bulk cell (LSC−) fraction of AML cells using a published database (Ng et al., 2016). MIA40/ALR substrates were enriched in LSCs compared with bulk AML cells (Figures S1A–S1C), MIA40 protein levels were increased in AML compared with normal hematopoietic cells (Figure S1E), and levels of ALR (GFER) protein and mRNA were similar (Figures S1C and S1E). By interrogating the published BloodSpot database (Bagger et al., 2019) ALR expression was higher in normal hematopoietic stem and progenitor cells compared with more differentiated cells (Figure S1D). No gain-of-function mutations for MIA40 and ALR were reported in AML samples (Ley et al., 2013; Tyner et al., 2018).

Next, we evaluated the importance of the MIA pathway in AML and LSCs by targeting the sulfhydryl oxidase ALR. We knocked down ALR in OCI-AML2, NB4, and TEX AML cells. ALR knockdown reduced the growth and viability of these cells (Figure 1A). As leukemia-initiating stem cells are implicated in disease relapse (Pollyea and Jordan, 2017; Kreso and Dick, 2014), we explored the importance of ALR in TEX cells that are arranged in a hierarchy of stem and bulk cells (Warner et al., 2005). After transduction with short hairpin RNA (shRNA) targeting ALR, but prior to the onset of cell death, equal numbers of TEX cells were injected into the femur of sub-lethally irradiated NOD/SCID-GF mice. Six weeks later, the percentage of human AML cells was quantified in the non-injected femur by flow cytometry. Knockdown of ALR targeted the leukemia-initiating cells, as demonstrated by reduced engraftment of TEX cells (Figure 1B). Moreover, mice engrafted with ALR-deficient TEX cells survived longer than mice engrafted with wild-type TEX cells (Figure 1B).

To further evaluate the effects of ALR inhibition in AML, we used the selective ALR inhibitor MitoBloCK-6 (mitochondrial protein import blocker) (Dabir et al., 2013; Quirós et al., 2017). Similar to genetic knockdown of ALR, MitoBloCK-6 was cytotoxic to OCI-AML2, NB4, TEX, and Jurkat leukemia cells as measured by MTS assay (Figure 1C), CellTiter-Fluor (Figure S1G), and propidium iodide staining (Figure S1G).

MitoBloCK-6 reduced the clonogenic growth of AML cells preferentially over normal hematopoietic cells (Figure 1D). ALR inhibition also preferentially reduced the frequency of AML stem/progenitor cells over normal hematopoietic stem cells, as measured by long-term culture-limiting dilution assays (Figure 1E). Moreover, inhibition of ALR with MitoBloCK-6 increased the differentiation of OCI-AML2 and NB4 cells, as measured by increased surface expression of the myeloid markers CD11b and CD14 (Figures 1F and 1G). Thus, the mitochondrial oxidase ALR regulates differentiation and stem cell-like properties of AML cells.

### Inhibition of ALR Targets AML Cells and Stem Cells *In Vivo*

Next, we assessed the efficacy and toxicity of targeting ALR in mouse models of leukemia. Mice engrafted with OCI-AML2 cells after ALR knockdown had decreased rates of tumor growth and longer survival compared with mice xenografted with wild-type cells (Figures 2A and S2A).

Furthermore, we evaluated the effect of pharmacological inhibition of ALR *in vivo*. Mice xenografted with OCI-AML2 cells were treated with MitoBloCK-6 (80 mg/kg intraperitoneally [i.p.] 5 of 7 days/twice daily) or vehicle control. MitoBloCK-6 reduced tumor growth (Figures 2B and S2C) without evidence of toxicity, as measured by body weight (Figure S2B), serum chemistry, and gross and histologic examination of the organs at the end of the experiment (Figures S2D and S2E).

We also evaluated the effects of ALR inhibition on primary AML cells *in vivo*. Primary AML cells were injected intra-femorally into sub-lethally irradiated NOD/SCID mice. Ten days after injection, mice were treated with MitoBloCK-6 or vehicle control (80 mg/kg twice daily). MitoBloCK-6 reduced the engraftment of AML cells into the mouse marrow (Figure 2C). Using serial transplants of AML cells harvested from the marrow of primary recipients into untreated secondary recipients, we showed that inhibiting ALR targeted LSCs (Figure 2D). In contrast, systemic treatment with MitoBloCK-6 did not reduce the engraftment of normal hematopoietic progenitor cells, suggesting preferential activity toward AML over normal hematopoietic cells (Figures 2E and S2F).

### Mitochondrial Copper Chaperone COX17 Is a Downstream Target of ALR and Its Depletion Phenocopies ALR Inhibition

The mitochondrial copper chaperone COX17 is a substrate of the MIA pathway and is folded into its mature form in the mitochondrial IMS by ALR and MIA40. When the folding of COX17 in the IMS is impaired, it exits the mitochondria and is degraded in the cytoplasm (Bragoszewski et al., 2015). Therefore, we evaluated the effects of ALR inhibition on levels of COX17. Genetic or chemical inhibition of ALR reduced levels of COX17 in the mitochondria (Figures 3A and 3B). In contrast, few or no reductions were observed in other substrates of the MIA pathway, including TIMM23, TIMM22, TIM9, SOD1 (CCS), and TIMM10 (Figures 3A and 3B). We confirmed reductions in COX17 after ALR inhibition by confocal microscopy. Under basal untreated conditions, COX17 localized to the mitochondria as expected (Figure S3A). Upon inhibition of ALR, mitochondrial COX17 decreased, and cytoplasmic levels were slightly increased (Figure S3A), likely reflecting the degradation of misfolded proteins not retained in the IMS.

We measured the expression of COX17 protein in primary AML and normal hematopoietic cells using immunoblotting.

(F) CD11b expression in OCI-AML2 and NB4 leukemic cells after treatment with increasing concentrations of MitoBloCK-6.
(G) Expression of CD14 on OCI-AML2 cells after treatment with increasing concentrations of MitoBloCK-6.
Data represent mean ± SD. **$p < 0.01$, ***$p < 0.001$, and ****$p < 0.0001$ by Student's t test. Significance for survival was measured by log rank test. The p value for LTC-IC assay was calculated from chi-square score and degrees of freedom (DF).

Please cite this article in press as: Singh et al., Disrupting Mitochondrial Copper Distribution Inhibits Leukemic Stem Cell Self-Renewal, Cell Stem Cell (2020), https://doi.org/10.1016/j.stem.2020.04.010



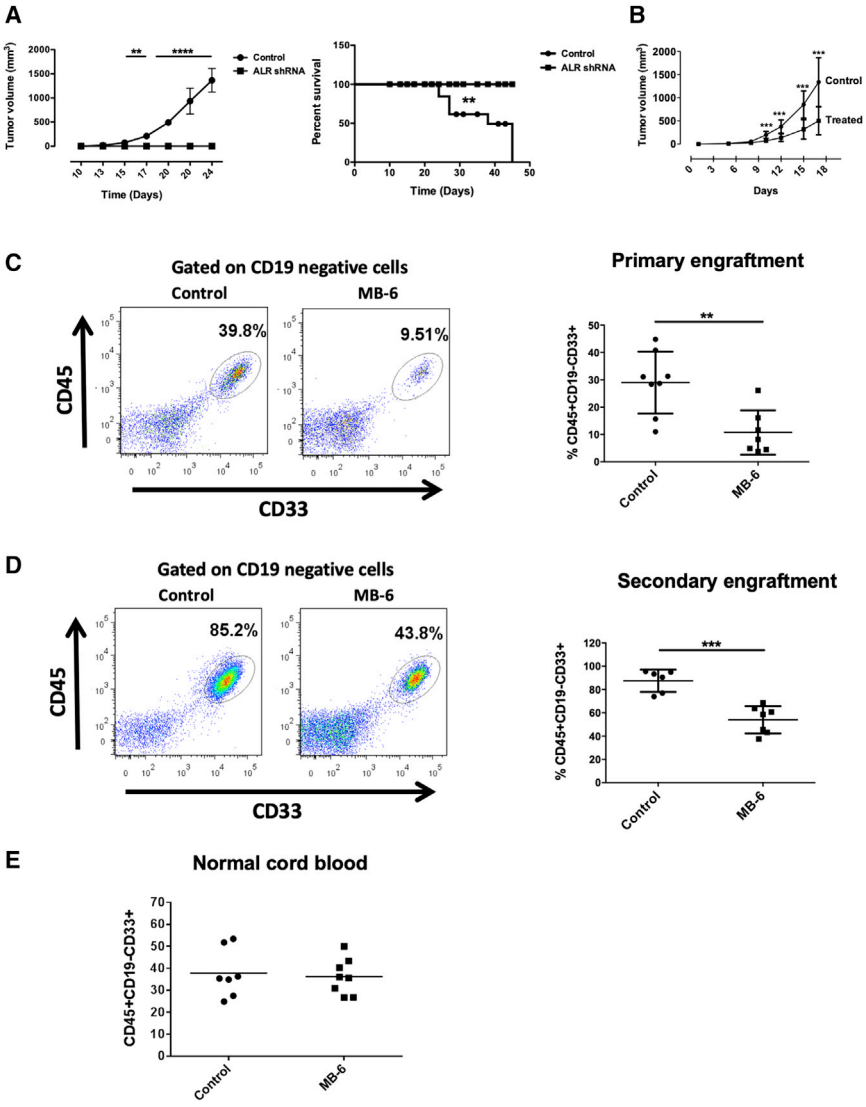


**Figure 2. Inhibition of ALR Targets AML Cells and Stem Cells *In Vivo***

(A) OCI-AML2 cells were transduced with shRNA targeting ALR or control sequences. Five days after transduction, cells were injected sub-cutaneously into flanks of SCID mice. Tumor volume was measured every other day for 3 weeks, 10 days after injection. Survival of mice was measured over a period of 45 days.

(B) OCI-AML2 cells were injected sub-cutaneously into flanks of SCID mice. Five days post-injection, mice were treated with MitoBloCK-6 (80 mg/kg i.p. 5 of 7 days/twice daily, 16 doses) or vehicle control. Tumor volume was measured over time.

(C) Primary AML cells were injected into the right femurs of sub-lethally irradiated NOD/SCID mice. Ten days after injection, mice were treated with vehicle or MitoBloCK-6 (80 mg/kg i.p. twice daily for 10 days, 20 doses). Representative fluorescence-activated cell sorting (FACS) plots of mice from control or treated groups and percentage human AML cells in the un-injected left femur are shown (patient ID AML 100214).

(D) Cells from (C) were injected into secondary untreated mice.

(E) Normal cord blood cells were injected into sub-lethally irradiated NOD/SCID-GF mice and treated with vehicle or MitoBloCK-6 as in (C).

Data represent mean ± SD. $^{**}p < 0.01$ and $^{***}p < 0.001$ by Student's t test. Significance for survival was measured by log rank test.

COX17 was higher in AML samples compared with normal hematopoietic cells (Figure S1E). COX17 gene expression was also higher in normal hematopoietic stem and progenitor cells compared with more differentiated hematopoietic cells (Figure S1F).

As inhibiting ALR led to a preferential reduction in COX17, we tested whether loss of COX17 phenocopied ALR depletion. Knockdown of COX17 reduced the growth and viability of OCI-AML2 cells (Figure 3C) and decreased the engraftment of TEX cells into the marrow of NOD/SCID-GF mice (Figure 3D). In addition, knockdown of COX17 in primary AML cells reduced their ability to engraft the marrow of immune-deficient mice (Figure 3E). Moreover, knockdown of COX17 increased AML differentiation, as evidenced by increased CD11b surface expression (Figure 3F). Thus, knockdown of COX17 mimics the effects of ALR inhibition.

COX17 is essential for loading copper onto the respiratory chain IV complex subunit, cytochrome *c* oxidase (Culotta et al., 1997; Glerum et al., 1996). Therefore, we measured the effects of COX17 and ALR inhibition on mitochondrial and respiratory chain function. We observed a slight but significant reduction in respiratory chain complex II and IV activity after knockdown of COX17, but the activities of the other respiratory chain complexes were not affected by COX17 or ALR inhibition (Figure S3E). However, this mild reduction in the activity of respiratory complexes did not result in functional inhibition of mitochondrial activity, as evidenced by unaltered basal oxygen consumption, unchanged intracellular ATP levels, and no increase in ROS production (Figures S4A–S4C and S4E). Inhibiting COX17 and ALR also did not change levels of Drp1, suggesting normal mitochondrial fission (Figure S4D).

## Redistribution of Mitochondrial Copper Decreases Levels of SAM and DNA Methylation

As COX17 and ALR inhibition did not significantly impair oxidative phosphorylation, we searched for other mechanisms by which inhibiting these targets would affect AML differentiation and stem cell function. COX17 is a metallochaperone and loads copper onto cytochrome *c* oxidase (Cobine et al., 2006; Takahashi et al., 2002). Therefore, we measured changes in mitochondrial copper using inductively coupled plasma mass spectrometry (ICP-MS). Inhibiting COX17 and ALR increased mitochondrial copper 7- and 2.5-fold, respectively (Figure 4A).

Copper binds and negatively regulates the activity of S-adenosylhomocysteine hydrolase (SAHH), a cytoplasmic and

Please cite this article in press as: Singh et al., Disrupting Mitochondrial Copper Distribution Inhibits Leukemic Stem Cell Self-Renewal, Cell Stem Cell (2020), https://doi.org/10.1016/j.stem.2020.04.010





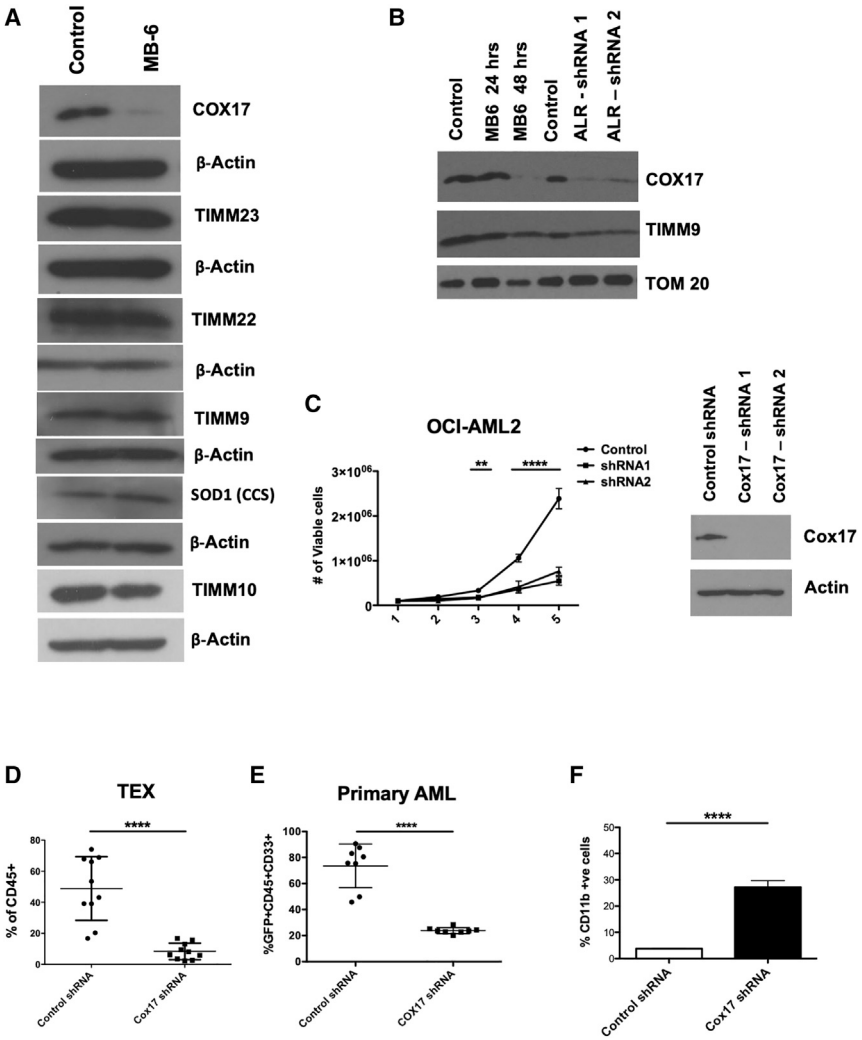


**Figure 3. Mitochondrial Copper Chaperone Cox17 Is a Downstream Target of ALR, and Its Depletion Phenocopies ALR Inhibition**

(A) OCI-AML2 cells were treated with MitoBloCK-6 (5 μM) for 72 h. Levels of COX17, TIMM23, TIM22, TIM9, SOD1 (CCS), TIM10, and β-actin were measured in whole-cell lysates by immunoblotting.

(B) Levels of COX17, TIMM9, and Tom 20 were measured by immunoblotting in lysates of mitochondria from OCI-AML2 cells treated with MitoBloCK-6 or after ALR knockdown with shRNA.

(C) OCI-AML2 cells were transduced with shRNA targeting COX17 or control sequences. Five days after transduction, levels of COX17 were measured by immunoblotting. Growth and viability were measured by trypan blue exclusion staining.

(D) TEX cells transduced with shRNA targeting COX17 or control sequence were injected into the right femur of NOD/SCID-GF mice. Five weeks post-injection, engraftment of TEX cells into the un-injected left femur of the mice was measured by flow cytometry.

(E) Primary AML cells were transduced with shRNA targeting COX17 or control sequence were injected into the right femur of NOD/SCID mice (patient ID AML 120287). Eight weeks post-injection, engraftment of AML into the un-injected left femur of the mice was measured by flow cytometry. Engraftment efficiency was normalized to transduction efficiency

(F) OCI-AML2 cells were transduced with shRNA targeting COX17 or control sequences. Five days after transduction, expression of CD11b was measured by flow cytometry.

Data represent mean ± SD. ****$p < 0.0001$ by Student's t test.

mitochondrial enzyme involved in the preservation of the SAM/S-adenosylhomocysteine (SAH) ratio in cells (Medici et al., 2013). SAM and SAH are metabolites that are important in the epigenetic regulation of stemness and differentiation (Fernández-Arroyo et al., 2016; Shlomi and Rabinowitz, 2013). Therefore, we examined whether ALR inhibition would affect SAHH enzymatic activity and discovered that ALR inhibition with MitoBloCK-6 decreased the intracellular enzymatic activity of SAHH (Figure 4C). In addition, inhibiting COX17 and ALR decreased intracellular levels of SAM (Figures 4D and S6J), a universal methyl donor that regulates DNA methylation (Robertson, 2005). We therefore evaluated the effects of COX17 and ALR inhibition on DNA methylation and determined that inhibiting COX17 and ALR decreased global DNA methylation (Figure 4E). In contrast, levels of histone H3K4, H3K36, and H3K79 methylation were not reduced (Figure S6D).

Of note, basal levels of copper trended higher in the CD34+ fraction of 8,227 cells compared with the bulk fraction (Figure S3B). Intracellular iron also increased after ALR inhibition (Figure S3C). However, this change did not seem functionally important as chelation of intracellular iron with deferiprone did not abrogate the effects of ALR inhibition (Figure S3D).

Inhibition of COX17 and ALR produced structural changes in the mitochondria with enlarged and disrupted cristae as well as vacuoles in the matrix (Figures 4B and S4F). These changes in mitochondrial morphology are similar to those reported in the copper overload syndrome Wilson disease (Zischka et al., 2011).

To understand the importance of changing SAM levels in AML, we knocked down SAHH in AML cells and observed reductions in levels of SAM, DNA methylation, and growth and viability (Figures S5A–S5D). Knockdown of SAHH also decreased engraftment of TEX cells into mouse marrow (Figure S5E). Thus, SAHH knockdown produces effects similar to inhibition of ALR and COX17.

## Mitochondrial Copper Regulates the Gene Expression Profile of AML Cells by Epigenetic Modulation

Next, we measured changes in gene expression after ALR inhibition by RNA sequencing. We compared changes in gene expression after ALR inhibition with published genetic signatures of leukemic and normal stem and bulk cells (van Galen et al., 2019; Ng et al., 2016). Inhibition of ALR shifted gene expression away from a stem cell signature and toward a differentiated

Please cite this article in press as: Singh et al., Disrupting Mitochondrial Copper Distribution Inhibits Leukemic Stem Cell Self-Renewal, Cell Stem Cell (2020), https://doi.org/10.1016/j.stem.2020.04.010



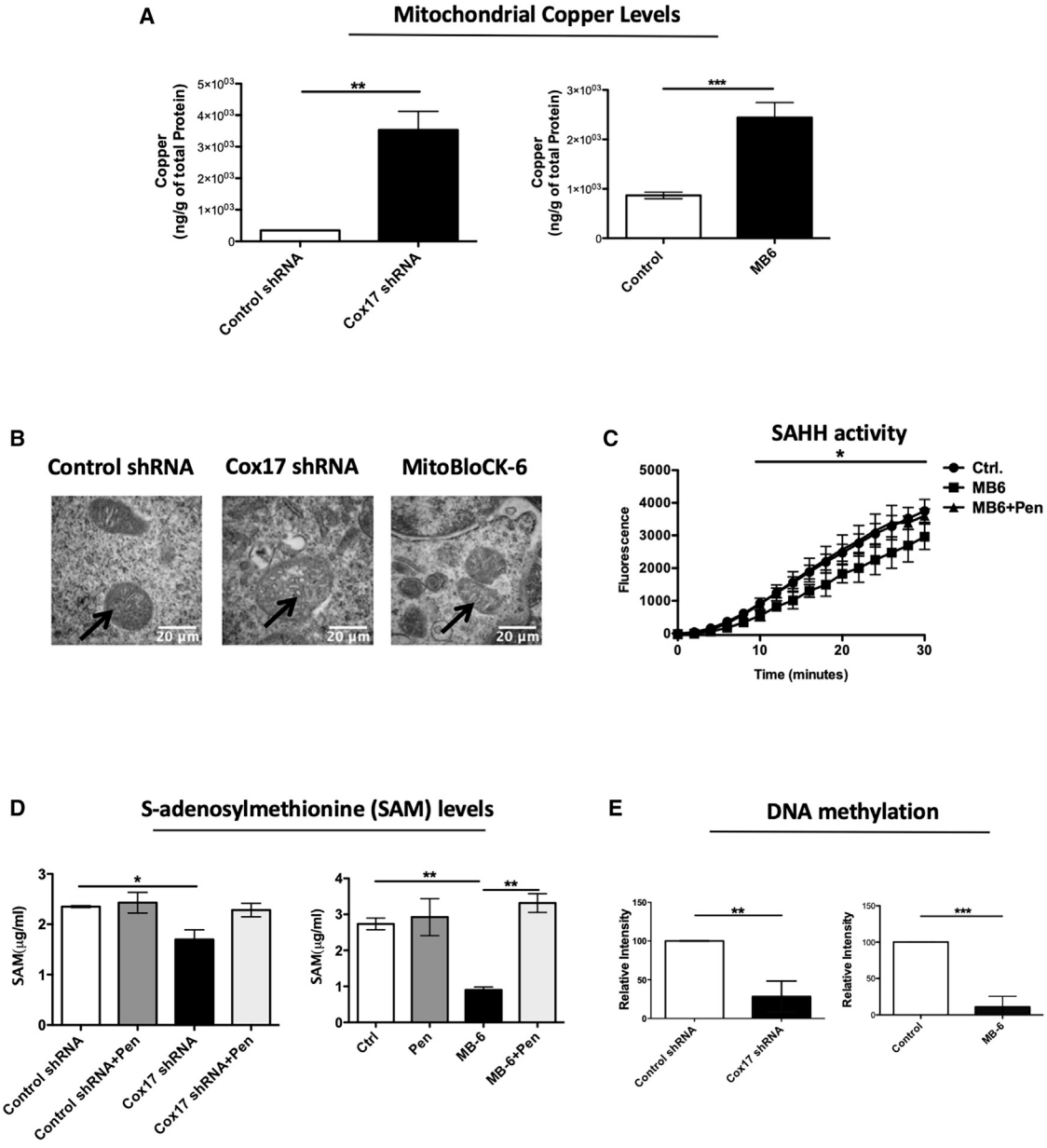


**Figure 4. Redistribution of Mitochondrial Copper Decreases Levels of S-Adenosylmethionine (SAM) and DNA Methylation**

(A) Levels of mitochondrial copper were measured by ICP-MS in OCI-AML2 cells after COX17 knockdown or treatment with MitoBloCK-6 (7.5 μM) for 48 s.

(B) Transmission electron micrographs of OCI-AML2 cells transduced with shRNA targeting COX17 or after treatment with MitoBloCK-6 (7.5 μM) for 48 h. Magnification 60,000×. Representative images are shown. Scale bar, 20 μM.

(C) The enzymatic activity of S-adenosylhomocysteine hydrolase (SAHH) was measured after treatment of OCI-AML2 cells with 4 μM MitoBloCK-6 and/or penicillamine (50 μM) (n = 4).

(D) Levels of S-adenosylmethionine (SAM) were measured in OCI-AML2 cells transduced with shRNA targeting COX 17 or treated with MitoBloCK-6 (7.5 μM) with and without penicillamine (25 μM).

(E) DNA methylation (5-methylcytosine) was measured in OCI-AML2 cells after COX17 knockdown or treatment with MitoBloCK-6 (7.5 μM).

Data represent mean ± SD. *p < 0.05, **p < 0.01, ***p < 0.001, and ****p < 0.0001 by Student's t test.

myeloid-like signature (Figures 5A and S6C). Pathways associated with myeloid differentiation, including immune response, interferon signaling, and cytokine stimulus (Figure 5C), were enriched after ALR inhibition, and similar pathways were enriched in the published datasets of bulk (LSC−) cells.

As global DNA methylation (Figure 4E) decreased after ALR inhibition, we sought to identify differentially methylated regions (DMRs) by performing DNA methylation sequencing after ALR inhibition. Control and MitoBloCK-6 treated samples separated in CpG methylation clustering (Figure S6H). Consistent with our

Please cite this article in press as: Singh et al., Disrupting Mitochondrial Copper Distribution Inhibits Leukemic Stem Cell Self-Renewal, Cell Stem Cell (2020), https://doi.org/10.1016/j.stem.2020.04.010





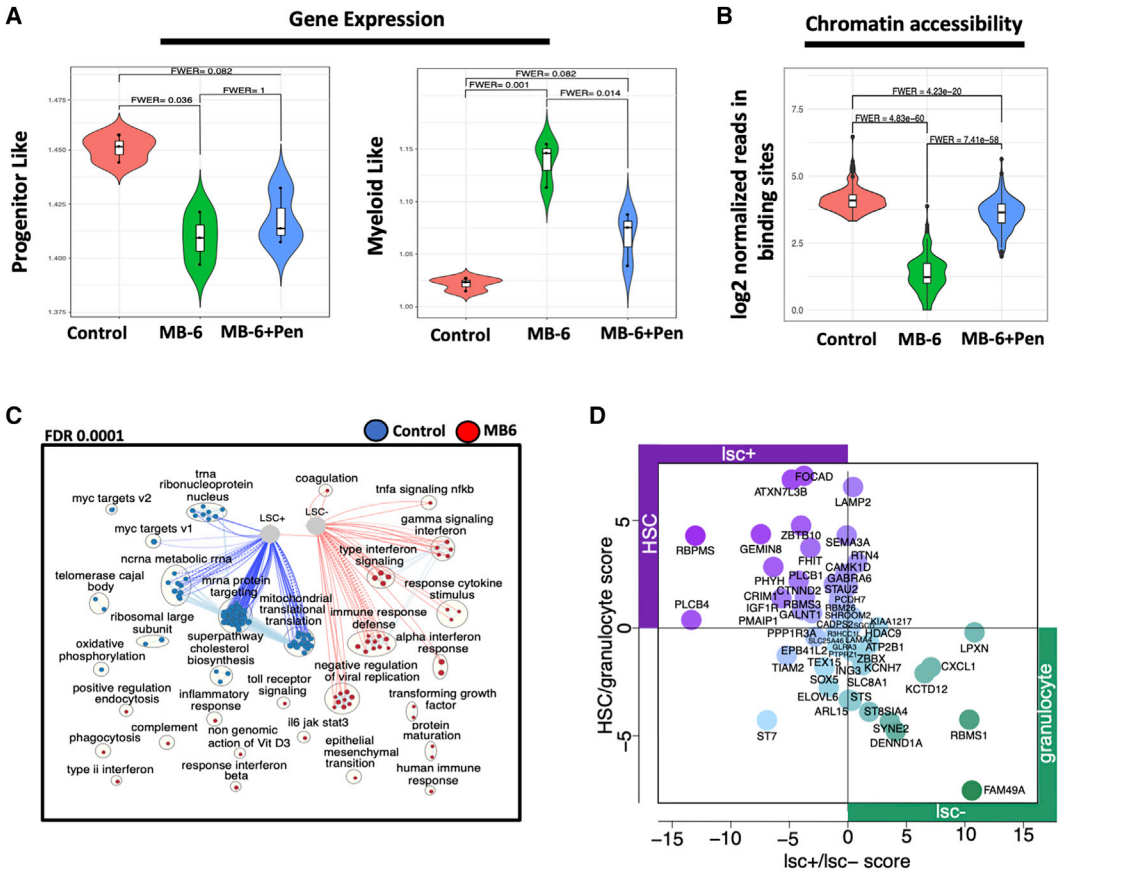


**Figure 5. Mitochondrial Copper Regulates the Gene Expression Profile of AML Cells by Epigenetic Modulation**

(A) Enrichment score for progenitor or myeloid gene signatures in OCI-AML2 cells 48 h after treatment with MitoBloCK-6 (7.5 μM) with or without co-treatment with 25 μM penicillamine for 48 h.

(B) Chromatin accessibility was measured by assay for transposase-accessible chromatin (ATAC) sequencing.

(C) Pathway enrichment map of genes differentially expressed after treatment with MitoBloCK-6 (7.5 μM). Pathway modules were labeled automatically using AutoAnnotate.

(D) Differential expression scores in LSC+/− and HSC/granulocytes of genes whose reduced accessibility was rescued by penicillamine.

(E) GO processes associated with hypomethylated genes identified by targeted DNA methylation sequencing.

Please cite this article in press as: Singh et al., Disrupting Mitochondrial Copper Distribution Inhibits Leukemic Stem Cell Self-Renewal, Cell Stem Cell (2020), https://doi.org/10.1016/j.stem.2020.04.010



findings above, the number of hypomethylated regions increased (18,452 new regions) after ALR inhibition (Figure S6I). Hypomethylated regions were enriched in Gene Ontology (GO) terms associated with differentiation, heterochromatin assembly, and heterochromatin organization (Figure 5E).

Considering the effect of ALR inhibition in differentiation, we determined if this also translated into changes in global chromatin accessibility (Cedar and Bergman, 2009; Farlik et al., 2016). Therefore, we performed assay for transposase-accessible chromatin using sequencing (ATAC-seq) after ALR inhibition. Inhibition of ALR reduced chromatin accessibility (Figures 5B, S6A, and S6B). Genes that were less accessible after ALR inhibition were enriched in the LSC+ signature genes (Figure 5D). Genes that were less accessible after ALR inhibition were distributed equally across all chromosomes (Figure S6G). These findings are in keeping with our observation that ALR inhibition promotes differentiation and decreases stem cell properties and prior studies showing stem cells have more accessible chromatin (Frey et al., 2017; Stergachis et al., 2013).

Daunorubicin is a chemotherapeutic agent that intercalates into DNA, increasing damage (Rabbani et al., 2005). Consistent with the reduced chromatin accessibility after ALR inhibition, the combination of daunorubicin and MitoBloCK-6 was antagonistic (Figure S6E). We also tested the combination of MitoBloCK-6 and the hypomethylating agents azacytidine and demonstrated additive reductions in cell growth and viability (Figure S6F).

### Copper Chelation by Penicillamine Rescues Effects of ALR Inhibition

Penicillamine is a copper chelator that forms an inactivating complex with Cu(II) ions (Peisach and Blumberg, 1969). Co-treatment of AML cells with penicillamine abrogated the effects of inhibiting COX17 and ALR and restored levels of SAM and SAHH activity toward basal levels (Figures 4C and 4D). Furthermore, co-treatment with penicillamine prevented the upregulation of CD11b and CD14 (cell surface markers associated with differentiation), prevented the shift in gene expression toward myeloid differentiation, and rescued alterations in chromatin accessibility (Figures 5A, 5B, 6A–6C, S6A, and S6B). The effects of ALR inhibition were not reversible, as the addition of penicillamine after treatment with MitoBloCK-6 did not reverse the effects of ALR inhibition on growth and viability (Figure S6K). Finally, co-treatment with penicillamine rescued the reductions in growth and viability seen after COX17 and ALR inhibition (Figures 6D and 6E).

## DISCUSSION

The vast majority of mitochondrial proteins are encoded by nuclear DNA, translated in the cytoplasm and imported into the mitochondria. Precursor proteins with specific import signals are imported into the sub-compartments of mitochondria through different protein channels and chaperones. Proteins traverse the mitochondrial outer membrane through the TOM complex. Once through the outer membrane, proteins destined for the inner mitochondrial membrane pass through the TIM22 complex, while proteins localized to the mitochondrial matrix use the TIM23 channel (Wiedemann and Pfanner, 2017). A subset of cysteine-rich peptides are folded into their mature forms and retained in the IMS through a process of oxidation and disulfide bond formation via the MIA/ALR pathway (Chacinska et al., 2004; Stojanovski et al., 2008). Here, we showed that modulation of MIA pathway by genetic or pharmacological inhibition of ALR promoted differentiation and decreased stem-like properties of AML cells through epigenetic changes caused by the redistribution of mitochondrial copper.

Our discovery that ALR regulates AML stem cells and differentiation is consistent with prior reports on the role of ALR in embryonic stem cells. In murine embryonic stem cells, inhibiting ALR decreased pluripotency (Ramalho-Santos et al., 2002; Todd et al., 2010). In these cells, loss of pluripotency was due to increased mitochondrial fission mediated by Drp1 (Todd et al., 2010). Although we observed reduced stem cell function and increased differentiation after inhibiting ALR in AML, we did not detect alterations in mitochondrial dynamics or regulators of mitochondrial fission. Rather, ALR regulated AML stem cell function through COX17 and mitochondrial copper.

COX17 is a cysteine-containing copper chaperone that is folded into its mature form in the mitochondrial IMS. When the folding of COX17 is impaired, the protein diffuses out of the mitochondria and is degraded in the cytoplasm (Bragoszewski et al., 2015). In our study, loss of COX17 phenocopied the effects of ALR inhibition.

Inhibition of ALR and COX17 decreased properties of AML stem cells by redistributing mitochondrial copper. Copper is a transition metal essential for proper cellular function. Copper enters cells primarily via the Ctr1 permease that spans the plasma membrane (Xu et al., 2013). Once inside the cell, copper is bound to chaperones such as COX17 that deliver the metal to target proteins (Xu et al., 2013). Of note, all intracellular copper is protein bound, as free ionic copper is highly toxic (Rae et al., 1999). The mitochondrial matrix, along with the Golgi and endoplasmic reticulum, is a major cellular reservoir for intracellular copper. Copper enters the mitochondria via the SLC25A3 transporter in yeast, but the mechanisms of copper import into the mitochondria of mammalian cells are not fully defined (Leary et al., 2009). Once inside the mitochondria, copper is transferred to proteins, including superoxide dismutase and cytochrome *c* oxidase, that use the metal as a cofactor for their biological activity (Leary et al., 2009).

SAHH is a copper-regulated enzyme. SAHH controls the conversion of SAH to adenosine and homocysteine and regulates levels of SAH and the methyl donor SAM. Thus, SAHH regulates cellular methylation. When copper binds SAHH, NAD+ cofactors are released, resulting in loss of its catalytic activity (Li et al., 2007). Inhibiting SAHH leads to decreased levels of SAM and decreased DNA methylation (Medici et al., 2013). Wilson disease is a hereditary disorder due to heterozygote mutations in the copper transporter ATP7b. In murine models of Wilson disease, the accumulation of copper leads to decreased SAHH enzymatic activity and lower levels of SAM with a resultant loss of DNA methylation. Changes in SAM and DNA methylation were rescued with the copper chelator penicillamine (Medici et al., 2013). Patients with Wilson disease experience hemolytic anemia due to copper accumulation and toxicity in erythrocytes, but hematopoiesis remains normal (El-Youssef, 2003; Rau et al., 2014). These results support our findings that increased

Please cite this article in press as: Singh et al., Disrupting Mitochondrial Copper Distribution Inhibits Leukemic Stem Cell Self-Renewal, Cell Stem Cell (2020), https://doi.org/10.1016/j.stem.2020.04.010



CellPress

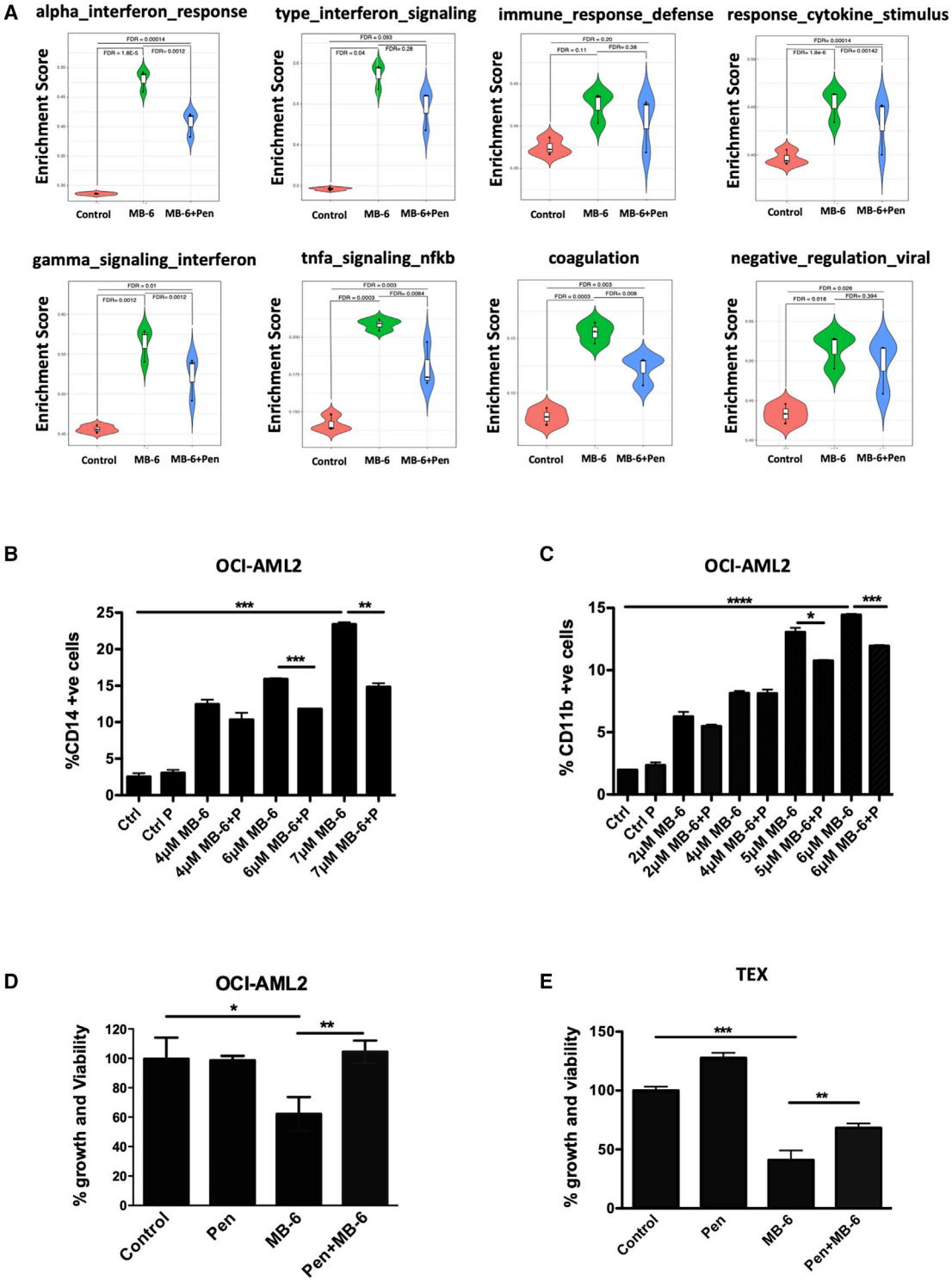


**Figure 6. Copper Chelation by Penicillamine Rescues Effects of ALR Inhibition**

(A) Pathway enrichment scores in OCI-AML2 cells treated with MitoBloCK-6 (7.5 μM) with or without penicillamine (25 μM).

(B) Surface expression of CD14 was measured in OCI-AML2 cells by flow cytometry 48 h after MitoBloCK-6 treatment with or without penicillamine (25 μM).

(C) Surface expression of CD11b was assessed similar to (B).

(D) OCI-AML2 cells were treated with 7.5 μM MitoBloCK-6 and/or penicillamine (25 μM) for 48 h. Cell growth and viability was measured by MTS assay.

(E) TEX cells were treated with 7.5 μM MitoBloCK-6 and/or penicillamine (25 μM) for 72 h. Cell growth and viability was measured by MTS assay.

Data represent mean ± SD. *p < 0.05, **p < 0.01, ***p < 0.001, and ****p < 0.0001 by Student's t test.

mitochondrial copper has preferential effects on AML cells compared with normal hematopoietic cells. However, we acknowledge that we could not determine whether the primary effect of ALR inhibition and copper accumulation was on DNA methylation or chromatin accessibility. We hypothesize that ALR inhibition and copper accumulation primarily affects DNA methylation and gene expression, while changes in chromatin accessibility are a secondary effect.

In conclusion, we describe a mechanism by which the mitochondrial sulfhydryl oxidase ALR and the copper chaperone COX17 regulate AML stem cell properties and differentiation by controlling the levels and distribution of mitochondrial copper. Thus, we highlight a new mechanism by which mitochondrial pathways control epigenetic changes and gene expression.

## STAR★METHODS

Detailed methods are provided in the online version of this paper and include the following:



## SUPPLEMENTAL INFORMATION

Supplemental Information can be found online at https://doi.org/10.1016/j.stem.2020.04.010.

## ACKNOWLEDGMENTS

We thank Jill Flewelling (Princess Margaret Cancer Center) for administrative assistance. We thank the Microscopy Imaging Laboratory at Sick Kids, Toronto, for performing electron microscopy. We also thank Monika Sharma, Zhibin Lu, and Neke Ibeh (Princess Margaret Cancer Centre, Toronto, Ontario, Canada) for help with the ATAC-seq and data analysis. We would like to thank Colin Bradley, Shane Stefan, Maria McCann, and Elvira Choperena (Victoria Hospital, London, Ontario, Canada) for help with copper measurements using ICP-MS. We would like to thank Olga Gan and Amanda Mitchell (Princess Margaret Cancer Centre, Toronto, Ontario, Canada) for help with the long-term culture-initiating cell (LTC-IC) assay. We thank the Leukemia Tissue Bank at Princess Margaret Cancer Centre/University Health Network, the source for primary AML samples. This work was supported by the Canadian Institutes of Health Research, the Ontario Institute of Cancer Research with funding provided by the Ontario Ministry of Research and Innovation, the Princess Margaret Cancer Centre Foundation, and the Ministry of Long Term Health and Planning in the province of Ontario. A.D.S. holds the Barbara Baker Chair in Leukemia and Related Diseases.

## AUTHOR CONTRIBUTIONS

Conception and Design, Collection, and/or Assembly of Data, Data Analysis, Interpretation, and Manuscript Writing, R.P.S. and D.V.J.; Collection and/or Assembly of Data, Data Analysis, and Interpretation, A.D.S.; Conception and Design, Financial Support, Collection and/or Assembly of Data, Data Analysis and Interpretation, Manuscript Writing, and Final Approval of the Manuscript, V.V., R.P.S., C.X., J.R.H., S.H.B., D.H.K., M.G., X.W., Y.J., D.S., S.L., N.M., A.K.S., S.M., A.B., G.E.T., J.S., E.O., M.D.M., A.A., S.M.C., G.D.B., and M.L.

## DECLARATION OF INTERESTS

A.D.S. has received honoraria or consulting fees from Novartis, Jazz, Otsuka, and Takeda Pharmaceuticals and research support from Medivir AB and Takeda. A.D.S. owns stock in Abbvie Pharmaceuticals and is named on a patent application for the use of DNT cells for the treatment of leukemia. D.V.J is currently an employee of Celgene/Bristol-Myers Squibb (BMS). M.D.M. has received consulting fees from Astellas, Abbvie, Celgene/BMS, and GlaxoSmithKline (GSK). S.M.C. has received honoraria from Celgene and Agios. S.M.C. has received research funding from Agios, Celgene, and Abbvie Pharmaceuticals.

Received: May 3, 2019
Revised: February 27, 2020
Accepted: April 15, 2020
Published: May 14, 2020

## REFERENCES

Bagger, F.O., Kinalis, S., and Rapin, N. (2019). BloodSpot: a database of healthy and malignant haematopoiesis updated with purified and single cell mRNA sequencing profiles. Nucleic Acids Res. *47* (D1), D881–D885.

Borisy, A.A., Elliott, P.J., Hurst, N.W., Lee, M.S., Lehár, J., Price, E.R., Serbedzija, G., Zimmermann, G.R., Foley, M.A., Stockwell, B.R., and Keith, C.T. (2003). Systematic discovery of multicomponent therapeutics. Proc. Natl. Acad. Sci. U S A *100*, 7977–7982.

Bragoszewski, P., Wasilewski, M., Sakowska, P., Gornicka, A., Böttinger, L., Qiu, J., Wiedemann, N., and Chacinska, A. (2015). Retro-translocation of mitochondrial intermembrane space proteins. Proc. Natl. Acad. Sci. USA *112*, 7713–7718.

Cedar, H., and Bergman, Y. (2009). Linking DNA methylation and histone modification: patterns and paradigms. Nat. Rev. Genet. *10*, 295–304.

Chacinska, A., Pfannschmidt, S., Wiedemann, N., Kozjak, V., Sanjuán Szklarz, L.K., Schulze-Specking, A., Truscott, K.N., Guiard, B., Meisinger, C., and Pfanner, N. (2004). Essential role of Mia40 in import and assembly of mitochondrial intermembrane space proteins. EMBO J. *23*, 3735–3746.

Chan, S.M., Thomas, D., Corces-Zimmerman, M.R., Xavy, S., Rastogi, S., Hong, W.J., Zhao, F., Medeiros, B.C., Tyvoll, D.A., and Majeti, R. (2015). Isocitrate dehydrogenase 1 and 2 mutations induce BCL-2 dependence in acute myeloid leukemia. Nat. Med. *21*, 178–184.

Chen, E.Y., Tan, C.M., Kou, Y., Duan, Q., Wang, Z., Meirelles, G.V., Clark, N.R., and Ma'ayan, A. (2013). Enrichr: interactive and collaborative HTML5 gene list enrichment analysis tool. BMC Bioinformatics *14*, 128.

Cobine, P.A., Pierrel, F., and Winge, D.R. (2006). Copper trafficking to the mitochondrion and assembly of copper metalloenzymes. Biochim. Biophys. Acta *1763*, 759–772.

Cole, A., Wang, Z., Coyaud, E., Voisin, V., Gronda, M., Jitkova, Y., Mattson, R., Hurren, R., Babovic, S., Maclean, N., et al. (2015). Inhibition of the mitochondrial protease ClpP as a therapeutic strategy for human acute myeloid leukemia. Cancer Cell *27*, 864–876.

Corces, M.R., Trevino, A.E., Hamilton, E.G., Greenside, P.G., Sinnott-Armstrong, N.A., Vesuna, S., Satpathy, A.T., Rubin, A.J., Montine, K.S., Wu, B., et al. (2017). An improved ATAC-seq protocol reduces background and enables interrogation of frozen tissues. Nat. Methods *14*, 959–962.

Culotta, V.C., Klomp, L.W.J., Strain, J., Casareno, R.L.B., Krems, B., and Gitlin, J.D. (1997). The copper chaperone for superoxide dismutase. J. Biol. Chem. *272*, 23469–23473.

Dabir, D.V., Hasson, S.A., Setoguchi, K., Johnson, M.E., Wongkongkathep, P., Douglas, C.J., Zimmerman, J., Damoiseaux, R., Teitell, M.A., and Koehler, C.M. (2013). A small molecule inhibitor of redox-regulated protein translocation into mitochondria. Dev. Cell *25*, 81–92.

El-Youssef, M. (2003). Wilson disease. Mayo Clin. Proc. *78*, 1126–1136.

Farlik, M., Halbritter, F., Müller, F., Choudry, F.A., Ebert, P., Klughammer, J., Farrow, S., Santoro, A., Ciaurro, V., Mathur, A., et al. (2016). DNA methylation dynamics of human hematopoietic stem cell differentiation. Cell Stem Cell *19*, 808–822.

Fernández-Arroyo, S., Cuyàs, E., Bosch-Barrera, J., Alarcón, T., Joven, J., and Menendez, J.A. (2016). Activation of the methylation cycle in cells reprogrammed into a stem cell-like state. Oncoscience *2*, 958–967.

Frey, W.D., Chaudhry, A., Slepicka, P.F., Ouellette, A.M., Kirberger, S.E., Pomerantz, W.C.K., Hannon, G.J., and Dos Santos, C.O. (2017). BPTF maintains chromatin accessibility and the self-renewal capacity of mammary gland stem cells. Stem Cell Reports *9*, 23–31.

Glerum, D.M., Shtanko, A., and Tzagoloff, A. (1996). Characterization of COX17, a yeast gene involved in copper metabolism and assembly of cytochrome oxidase. J. Biol. Chem. *271*, 14504–14509.

Hu, Y., and Smyth, G.K. (2009). ELDA: extreme limiting dilution analysis for comparing depleted and enriched populations in stem cell and other assays. J. Immunol. Methods. *347*, 70–78.

Itoh, K., Tezuka, H., Sakoda, H., Konno, M., Nagata, K., Uchiyama, T., Uchino, H., and Mori, K.J. (1989). Reproducible establishment of hemopoietic supportive stromal cell lines from murine bone marrow. Exp. Hematol. *17*, 145–153.

Kacmarczyk, T.J., Fall, M.P., Zhang, X., Xin, Y., Li, Y., Alonso, A., and Betel, D. (2018). "Same difference": comprehensive evaluation of four DNA methylation measurement platforms. Epigenetics Chromatin *11*, 21.

Kreso, A., and Dick, J.E. (2014). Evolution of the cancer stem cell model. Cell Stem Cell *14*, 275–291.

Krueger, F., and Andrews, S.R. (2011). Bismark: a flexible aligner and methylation caller for Bisulfite-Seq applications. Bioinformatics *27*, 1571–1572.

Kuleshov, M.V., Jones, M.R., Rouillard, A.D., Fernandez, N.F., Duan, Q., Wang, Z., Koplev, S., Jenkins, S.L., Jagodnik, K.M., Lachmann, A., et al. (2016). Enrichr: a comprehensive gene set enrichment analysis web server 2016 update. Nucleic Acids Res. *44* (W1), W90–W97.

Lagadinou, E.D., Sach, A., Callahan, K., Rossi, R.M., Neering, S.J., Minhajuddin, M., Ashton, J.M., Pei, S., Grose, V., O'Dwyer, K.M., et al. (2013). BCL-2 inhibition targets oxidative phosphorylation and selectively eradicates quiescent human leukemia stem cells. Cell Stem Cell *12*, 329–341.

Langmead, B., and Salzberg, S.L. (2012). Fast gapped-read alignment with Bowtie 2. Nat. Methods *9*, 357–359.

Leary, S.C., Winge, D.R., and Cobine, P.A. (2009). "Pulling the plug" on cellular copper: the role of mitochondria in copper export. Biochim. Biophys. Acta *1793*, 146–153.

Lechman, E.R., Gentner, B., Ng, S.W.K., Schoof, E.M., van Galen, P., Kennedy, J.A., Nucera, S., Ciceri, F., Kaufmann, K.B., Takayama, N., et al. (2016). miR-126 Regulates Distinct Self-Renewal Outcomes in Normal and Malignant Hematopoietic Stem Cells. Cancer Cell *29*, 602–606.

Ley, T.J., Miller, C., Ding, L., Raphael, B.J., Mungall, A.J., Robertson, A., Hoadley, K., Triche, T.J., Jr., Laird, P.W., Baty, J.D., et al.; Cancer Genome Atlas Research Network (2013). Genomic and epigenomic landscapes of adult de novo acute myeloid leukemia. N. Engl. J. Med. *368*, 2059–2074.

Li, H., Handsaker, B., Wysoker, A., Fennell, T., Ruan, J., Homer, N., Marth, G., Abecasis, G., and Durbin, R.; 1000 Genome Project Data Processing Subgroup (2009). The Sequence Alignment/Map format and SAMtools. Bioinformatics *25*, 2078–2079.

Li, M., Li, Y., Chen, J., Wei, W., Pan, X., Liu, J., Liu, Q., Leu, W., Zhang, L., Yang, X., et al. (2007). Copper ions inhibit S-adenosylhomocysteine hydrolase by causing dissociation of NAD+ cofactor. Biochemistry *46*, 11451–11458.

McLean, C.Y., Bristor, D., Hiller, M., Clarke, S.L., Schaar, B.T., Lowe, C.B., Wenger, A.M., and Bejerano, G. (2010). GREAT improves functional interpretation of cis-regulatory regions. Nat. Biotechnol. *28*, 495–501.

Medici, V., Shibata, N.M., Kharbanda, K.K., LaSalle, J.M., Woods, R., Liu, S., Engelberg, J.A., Devaraj, S., Török, N.J., Jiang, J.X., et al. (2013). Wilson's disease: changes in methionine metabolism and inflammation affect global DNA methylation in early liver disease. Hepatology *57*, 555–565.

Moffat, J., Grueneberg, D.A., Yang, X., Kim, S.Y., Kloepfer, A.M., Hinkle, G., Piqani, B., Eisenhaure, T.M., Luo, B., Grenier, J.K., et al. (2006). A lentiviral RNAi library for human and mouse genes applied to an arrayed viral high-content screen. Cell *124*, 1283–1298.

Mordas, A., and Tokatlidis, K. (2015). The MIA pathway: a key regulator of mitochondrial oxidative protein folding and biogenesis. Acc. Chem. Res. *48*, 2191–2199.

Nalesnik, M.A., Gandhi, C.R., and Starzl, T.E. (2017). Augmenter of liver regeneration: a fundamental life protein. Hepatology *66*, 266–270.

Ng, S.W.K., Mitchell, A., Kennedy, J.A., Chen, W.C., McLeod, J., Ibrahimova, N., Arruda, A., Popescu, A., Gupta, V., Schimmer, A.D., et al. (2016). A 17-gene stemness score for rapid determination of risk in acute leukaemia. Nature *540*, 433–437.

Nicolini, F.E., Cashman, J.D., Hogge, D.E., Humphries, R.K., and Eaves, C.J. (2004). NOD/SCID mice engineered to express human IL-3, GM-CSF and Steel factor constitutively mobilize engrafted human progenitors and compromise human stem cell regeneration. Leukemia *18*, 341–347.

Novershtern, N., Subramanian, A., Lawton, L.N., Mak, R.H., Haining, W.N., McConkey, M.E., Habib, N., Yosef, N., Chang, C.Y., Shay, T., et al. (2011). Densely interconnected transcriptional circuits control cell states in human hematopoiesis. Cell *144*, 296–309.

Pei, S., Minhajuddin, M., Adane, B., Khan, N., Stevens, B.M., Mack, S.C., Lai, S., Rich, J.N., Inguva, A., Shannon, K.M., et al. (2018). AMPK/FIS1-Mediated Mitophagy Is Required for Self-Renewal of Human AML Stem Cells. Cell Stem Cell *23*, 86–100.

Peisach, J., and Blumberg, W.E. (1969). A mechanism for the action treatment of penicillamine disease in the of Wilson's disease. Mol. Pharmacol. *5*, 200–209.

Pollyea, D.A., and Jordan, C.T. (2017). Therapeutic targeting of acute myeloid leukemia stem cells. Blood *129*, 1627–1635.

Quinlan, A.R. (2014). BEDTools: the Swiss-Army tool for genome feature analysis. Curr. Protoc. Bioinform. *47*, 11.12.1–11.12.34.

Quirós, P.M., Prado, M.A., Zamboni, N., D'Amico, D., Williams, R.W., Finley, D., Gygi, S.P., and Auwerx, J. (2017). Multi-omics analysis identifies ATF4 as a key regulator of the mitochondrial stress response in mammals. J. Cell Biol. *216*, 2027–2045.

Rabbani, A., Finn, R.M., and Ausió, J. (2005). The anthracycline antibiotics: antitumor drugs that alter chromatin structure. BioEssays *27*, 50–56.

Rae, T.D., Schmidt, P.J., Pufahl, R.A., Culotta, V.C., and O'Halloran, T.V. (1999). Undetectable intracellular free copper: the requirement of a copper chaperone for superoxide dismutase. Science *284*, 805–808.

Ramalho-Santos, M., Yoon, S., Matsuzaki, Y., Mulligan, R.C., and Melton, D.A. (2002). Transcriptional profiling of embryonic and adult stem cells. Science *298*, 597–600.

Rau, A.R., Usha, M., Mallya, P., and Rau, A.T.K. (2014). Cytopenia and bone marrow dysplasia in a case of Wilson's disease. Indian J. Hematol. Blood Transfus. *30* (*Suppl 1*), 433–436.

Robertson, K.D. (2005). DNA methylation and human disease. Nat. Rev. Genet. *6*, 597–610.

Robinson, M.D., McCarthy, D.J., and Smyth, G.K. (2010). edgeR: a Bioconductor package for differential expression analysis of digital gene expression data. Bioinformatics *26*, 139–140.

Shlomi, T., and Rabinowitz, J.D. (2013). Metabolism: cancer mistunes methylation. Nat. Chem. Biol. *9*, 293–294.

Skrtić, M., Sriskanthadevan, S., Jhas, B., Gebbia, M., Wang, X., Wang, Z., Hurren, R., Jitkova, Y., Gronda, M., Maclean, N., et al. (2011). Inhibition of mitochondrial translation as a therapeutic strategy for human acute myeloid leukemia. Cancer Cell *20*, 674–688.

Sriskanthadevan, S., Jeyaraju, D.V., Chung, T.E., Prabha, S., Xu, W., Skrtic, M., Jhas, B., Hurren, R., Gronda, M., Wang, X., et al. (2015). AML cells have low spare reserve capacity in their respiratory chain that renders them susceptible to oxidative metabolic stress. Blood *125*, 2120–2130.

Stergachis, A.B., Neph, S., Reynolds, A., Humbert, R., Miller, B., Paige, S.L., Vernot, B., Cheng, J.B., Thurman, R.E., Sandstrom, R., et al. (2013). Developmental fate and cellular maturity encoded in human regulatory DNA landscapes. Cell *154*, 888–903.

Stojanovski, D., Müller, J.M., Milenkovic, D., Guiard, B., Pfanner, N., and Chacinska, A. (2008). The MIA system for protein import into the mitochondrial intermembrane space. Biochim. Biophys. Acta *1783*, 610–617.

Takahashi, Y., Kako, K., Kashiwabara, S.-I., Takehara, A., Inada, Y., Arai, H., Nakada, K., Kodama, H., Hayashi, J.-I., Baba, T., et al. (2002). Mammalian copper chaperone Cox17p has an essential role in activation of cytochrome c oxidase and embryonic development. Mol. Cell Biol. *22*, 7614–7621.

Tarasov, A., Vilella, A.J., Cuppen, E., Nijman, I.J., and Prins, P. (2015). Sambamba: fast processing of NGS alignment formats. Bioinformatics *31*, 2032–2034.

Todd, L.R., Damin, M.N., Gomathinayagam, R., Horn, S.R., Means, A.R., and Sankar, U. (2010). Growth factor erv1-like modulates Drp1 to preserve mitochondrial dynamics and function in mouse embryonic stem cells. Mol. Biol. Cell *21*, 1225–1236.

Tyner, J.W., Tognon, C.E., Bottomly, D., Wilmot, B., Kurtz, S.E., Savage, S.L., Long, N., Schultz, A.R., Traer, E., Abel, M., et al. (2018). Functional genomic landscape of acute myeloid leukaemia. Nature *562*, 526–531.

van Galen, P., Hovestadt, V., Wadsworth Ii, M.H., Hughes, T.K., Griffin, G.K., Battaglia, S., Verga, J.A., Stephansky, J., Pastika, T.J., Lombardi Story, J., et al. (2019). Single-cell RNA-seq reveals AML hierarchies relevant to disease progression and immunity. Cell *176*, 1265–1281.e24.

Wang, C., Curtis, J.E., Minden, M.D., and McCulloch, E.A. (1989). Expression of a retinoic acid receptor gene in myeloid leukemia cells. Leukemia *3*, 264–269.

Warner, J.K., Wang, J.C.Y., Takenaka, K., Doulatov, S., McKenzie, J.L., Harrington, L., and Dick, J.E. (2005). Direct evidence for cooperating genetic events in the leukemic transformation of normal human hematopoietic cells. Leukemia *19*, 1794–1805.

Wiedemann, N., and Pfanner, N. (2017). Mitochondrial machineries for protein import and assembly. Annu. Rev. Biochem. *86*, 685–714.

Xu, W., Barrientos, T., and Andrews, N.C. (2013). Iron and copper in mitochondrial diseases. Cell Metab. *17*, 319–328.

Zhang, Y., Liu, T., Meyer, C.A., Eeckhoute, J., Johnson, D.S., Bernstein, B.E., Nusbaum, C., Myers, R.M., Brown, M., Li, W., et al. (2008). Model-based analysis of ChIP-seq (MACS). Genome Biol. *9*, R137.

Zischka, H., Lichtmannegger, J., Schmitt, S., Jägemann, N., Schulz, S., Wartini, D., Jennen, L., Rust, C., Larochette, N., Galluzzi, L., et al. (2011). Liver mitochondrial membrane crosslinking and destruction in a rat model of Wilson disease. J. Clin. Invest. *121*, 1508–1518.

Please cite this article in press as: Singh et al., Disrupting Mitochondrial Copper Distribution Inhibits Leukemic Stem Cell Self-Renewal, Cell Stem Cell (2020), https://doi.org/10.1016/j.stem.2020.04.010



## STAR★METHODS

### KEY RESOURCES TABLE

| Reagents or Resource | Source | Identifier |
|---|---|---|
| Antibodies | | |
| Rabbit polyclonal anti GFER (ALR) | Proteintech | Cat# 11293-1-AP, RRID:AB_2109970 |
| FITC Mouse anti-human CD45 (2D1) | BD Biosciences | Cat# 347463, RRID:AB_400306 |
| PE Mouse anti-human CD45 (HI30) | BD Biosciences | Cat# 555483, RRID:AB_395875 |
| Mouse monoclonal anti beta-Actin (AC-15) | Santa Cruz Biotechnology | Cat# sc-69879, RRID:AB_1119529 |
| Rabbit polyclonal anti beta-Tubulin | Santa Cruz Biotechnology | Cat# sc-9104, RRID:AB_2241191 |
| APC Mouse anti-human CD11b (D12) | BD Biosciences | Cat# 340937, RRID:AB_400549 |
| APC Mouse anti-human CD14 (MøP9) | BD Biosciences | Cat# 555399, RRID:AB_398596 |
| Anti CD122 | Lab Stock | N/A |
| PE-Cy5 Mouse anti-human CD33 (WM53) | BD Biosciences | Cat# 551377, RRID:AB_394173 |
| PE anti-human CD19 (4G7) | BD Biosciences | Cat# 349209, RRID:AB_400407 |
| Rabbit polyclonal anti COX17 | Proteintech | Cat# 11464-1-AP, RRID:AB_2085109 |
| Rabbit polyclonal anti TIMM9 | Proteintech | Cat# 11479-1-AP, RRID:AB_2204698 |
| Rabbit polyclonal anti TIMM10 | Proteintech | Cat# 11124-2-AP, RRID:AB_2201981 |
| Rabbit polyclonal anti CCS | Proteintech | Cat# 22802-1-AP |
| Mouse anti TIMM23 (32/TIMM23) | BD Biosciences | Cat# 611223, RRID:AB_398755 |
| Rabbit polyclonal anti TIMM22 | Proteintech | Cat# 14927-1-AP, RRID:AB_11183050 |
| Mouse anti TOM20 (29/TOM20) | BD Biosciences | Cat# 6112278, RRID:AB_399595 |
| Rabbit polyclonal anti Drp1 | Millipore | Cat# ABT155, RRID:AB_11203145 |
| Rabbit polyclonal anti SAHH | Proteintech | Cat# 10757-2-AP, RRID:AB_2289488 |
| Rabbit anti H3 (trimethyl k4) (C42D8) | Cell Signaling | Cat# 9751 |
| Rabbit polyclonal anti H3 (trimethyl k36) | Abcam | Cat# ab9050, RRID:AB_306966 |
| Rabbit polyclonal anti H3 (trimethyl k79) | Abcam | Cat# ab2621, RRID:AB_303215 |
| Rabbit anti H3 (D1H2) | Cell Signaling | Cat# 4499, RRID:AB_10544537 |
| Rabbit polyclonal anti CHCHD4 | Proteintech | Cat# 21090-1-AP, RRID:AB_10734583 |
| Rabbit polyclonal anti 5-Hydroxymethylcytoseine | Active Motif | Cat# 39769, RRID:AB_10013602 |
| Mouse anti ds DNA (3519DNA) | Abcam | Cat# ab27156, RRID:AB_470907 |
| Biological Samples | | |
| Human AML Patient Samples (Patient ID in Table S1) | Leukemia tissue bank, Princess Margaret Cancer Centre/University Health Network. | N/A |
| Normal Peripheral Blood Stem cells (PBSCs) | Leukemia tissue bank, Princess Margaret Cancer Centre/University Health Network. | N/A |
| Chemicals, Peptides and Recombinant Proteins | | |
| Iscove's Modification Dulbecco's Modification Eagle's Medium (IMDMEM | Wisent | Cat# 319-701-CL |
| RPMI 1640 | Wisent | Cat# 350-700-CL |
| MyeloCult H5100 | STEMCELL Technologies | Cat# 05150 |
| X-VIVO 10 Chemically Defined, Serum-free Hematopoietic Cell Medium | Lonza | Cat# 04-380Q |
| Dulbecco's Modification Eagle's Medium (DMEM) | Wisent | Cat# 319-005-CL |
| Fetal Bovine Serum | Sigma-Aldrich | Cat# F1051 |
| Recombinant Human SCF Protein | R&D Systems | Cat# 255-sc/*cf.* |
| Recombinant Human IL-3 Protein | R&D Systems | Cat# 203-IL |
| L-Glutamine | ThermoFisher Scientific | Cat# 25030081 |

(*Continued on next page*)

Please cite this article in press as: Singh et al., Disrupting Mitochondrial Copper Distribution Inhibits Leukemic Stem Cell Self-Renewal, Cell Stem Cell (2020), https://doi.org/10.1016/j.stem.2020.04.010



*Continued*

| Reagents or Resource | Source | Identifier |
|---|---|---|
| Recombinant Human IL-3 | PeproTech | Cat# 200-03 |
| Recombinant Human SCF | PeproTech | Cat# 300-07 |
| Recombinant Human Flt3-Ligand | PeproTech | Cat# 300-19 |
| Recombinant Human TPO | PeproTech | Cat# 300-18 |
| Recombinant Human IL-6 | PeproTech | Cat# 200-06 |
| BIT 9500 Serum Substitute | STEMCELL Technologies | Cat# 09500 |
| Human GM-CSF | Miltenyi Biotec | Cat# 130-093-866 |
| Human IL-6 | Miltenyi Biotec | Cat# 130-095-365 |
| Human Flt3-Ligand | Miltenyi Biotec | Cat# 130-096-479 |
| Human IL-7 | Miltenyi Biotec | Cat# 130-095-363 |
| Granulocyte colony stimulating factor (G-CSF) | Amgen Canada | Cat# 121181-53-1 |
| Puromycin HCL | Sigma-Aldrich Cat# P8833 | Cat# P8833 |
| Protamine Sulfate | MP Biomedicals | Cat# 194729 |
| RIPA buffer | Lab Stock | N/A |
| TBS (10X) | Wisent | Cat# 311-030-LL |
| Thermo Scientific Pierce ECL western blotting substrate | ThermorFisher Scientific | Cat# PI32106 |
| Propidium Iodide | BioVision | Cat# 1056-1 |
| IBc buffer (10mM TRIS-MOPS, 1mM EGTA,0.2M Sucrose, pH 7.4) | Lab stock | N/A |
| Red Blood Cell Lysing Buffer Hybri-Max | Sigma-Aldrich | Cat# R7757 |
| UltraComp eBeads | affymetrix eBioscience | Cat# 01-2222-42 |
| Methanol | Bioshop | Cat# MET302 |
| Oligomycin | Sigma-Aldrich | Cat# 75351 |
| FCCP | Cayman Chemical | Cat# 15218 |
| Corning Cell-Tak | FisherScientific | Cat# C354240 |
| Seahorse XF assay medium | Agilent | Cat# 102365-100 |
| Paraformaldehyde | Electron Microscopy Sciences | Cat# RT19200 |
| 70% Glutaraldehyde | Electron Microscopy Sciences | Cat# 16360 |
| BSA | Sigma | Cat# A9647 |
| Triton X-100 | Sigma | Cat# T8787 |
| 1N Sodium Hydroxide [NaOH] | Lab stock | N/A |
| Osmium tetraoxide [OsO4] | Electron Microscopy Sciences | Cat# RT19100 |
| Embed-812 kit | Electron Microscopy Sciences | Cat# 14120 |
| 300 Mesh Copper grids | Electron Microscopy Sciences | Cat# G300H-Cu |
| Uranyl Acetate | Electron Microscopy Sciences | Cat# 22400 |
| Lead Nitrate [Pb(NO3)2] | Electron Microscopy Sciences | Cat# RT17900 |
| Sodium Citrate [Na3C6H5O7$2H2O] | Electron Microscopy Sciences | Cat# RT21140 |
| PBS | Wisenet | Cat# 311-010-CL |
| DMSO | Sigma | Cat# D8418 |
| 16% paraformaldehyde | Electron Microscopy Sciences | Cat# 15710 |
| SuperScript IV Reverse Transcriptase | ThermoFisher Scientific | Cat# 18090050 |
| CellTiter 96 Aqueous MTS Reagent Powder | Promega | Cat# G1111 |
| RetroNectin Recombinant Human Fibronectin Fragment | Takara | Cat# T100A |
| Phosphate Buffered Saline (DPBS1X) | ThermoFisher Scientific | Cat# 14190144 |
| Lysis buffer (10 mM Tris-HCl, pH 7.4, 10 mM NaCl, 3 mM $MgCl_2$, 0.1% IGEPAL CA-630) | Lab Stock | N/A |
| 2x TD (2x reaction buffer) | Illumina | Cat# FC-121-1030 |
| TDE1 (Nextera Tn5 Transposase) | Illumina | Cat# FC-121-1030 |

(*Continued on next page*)

Please cite this article in press as: Singh et al., Disrupting Mitochondrial Copper Distribution Inhibits Leukemic Stem Cell Self-Renewal, Cell Stem Cell (2020), https://doi.org/10.1016/j.stem.2020.04.010





*Continued*

| Reagents or Resource | Source | Identifier |
|---|---|---|
| NEBNext High-Fidelity 2x PCR Master Mix | New England Labs | Cat# M0541 |
| 100x SYBR Green I | Invitrogen | Cat# S-7563 |
| 30% Acrylamide | BioRad | Cat# 1610156 |
| Ammonium Persulfate | Sigma | Cat# A3678 |
| Nitrocellulose Membrane (0.2μM) | GE healthcare (Amersham) | Cat# 45004001 |
| Immobilon-FL Membrane (0.45μM) | Millipore | Cat# IPFL00010 |
| Immobilon-pSQ Membrane (0.45μM) | Millipore | Cat# ISEQ00010 |
| MitoBlock-6 | Millipore | Cat# 5.05759.0001 |
| D-Penicillamine | Sigma | Cat# P4875 |
| Critical Commercial Assays | | |
| CellTiter-Flour | Promega | Cat# G6082 |
| E.N.Z.A Plasmid Midi Kit | Omega BIO-TEK | Cat# D6904-04 |
| Protein Assay Dye | Bio-Rad | Cat# 5000006 |
| DC Protein Assay kit II | Bio-Rad | Cat# 5000112 |
| MethoCult H4100 | STEMCELL Technologies | Cat# 04100 |
| MethoCult H4434 | STEMCELL Technologies | Cat# 04434 |
| MethoCult GF M3534 | STEMCELL Technologies | Cat# 03534 |
| Bioanalyzer RNA Analysis Kit | Agilent Technologies | Cat# 5067-1511 |
| MinElute PCR Purification Kit | QIAGEN | Cat# 28004 |
| TruSeq® Stranded Total RNA Library Prep | Illumina | Cat# 20020596 |
| TruSeq-Methyl Capture EPIC Library Prep Kit | Illumina | Cat# FC-151-1002 |
| RNeasy Plus Mini Kit | QIAGEN | Cat# 74134 |
| SAM Eliza Kit | Cell Biolabs | Cat# STA-672 |
| SAHH activity kit | Abcam | Cat# ab197002 |
| Lenti-X Concentrator | Takara | Cat# 631231 |
| Deposited Data | | |
| Gene expression profiling by high throughput sequencing (RNA seq) | This paper | GEO: GSE146252 |
| Methylation profiling by high throughput sequencing (Cap Meth seq) | This paper | GEO: GSE146252 |
| Genome binding/occupancy profiling by high throughput sequencing (ATAC seq) | This paper | GEO: GSE146252 |
| Experimental Models: Cell Lines | | |
| Human: OCI-AML2 | Wang et al., 1989 | N/A |
| Human: TEX | Warner et al., 2005 | N/A |
| Human: NB4 | | N/A |
| Human: Jurkat | ATCC | TIB-152 |
| 8227 | Lechman et al., 2016 | N/A |
| MS-5 Stroam cells | Itoh et al., 1989 | N/A |
| Experimental Models: Organisms/Strains | | |
| Mouse: NOD.Cg-Prkdc$^{scid}$ Il2rg$^{tm1Wjl}$ Tg(CMV-IL3,CSF2,KITLG)1Eav/MloySzJ (NOD-SCID-GF) | Nicolini et al., 2004 | N/A |
| Mouse: NOD.CB17-Prkdc$^{scid}$/J (NOD-SCID) | Jackson Laboratory | Cat# 001303, RRID: IMSR_JAX:001303 |
| Mouse: Prkdc$^{scid}$ (SCID) | In house | RRID: IMSR_ARC:SCID |
| Oligonucleotides | | |
| shRNAs targeting GFER (ALR), COX17, SAHH and control sequences | Refer to Table | Table S2 |
| Recombinant DNA | | |
| pLKO.1-Puro-shRNA lentiviral plasmid | Moffat et al., 2006 | N/A |
| pRS19-Puro-GFP-shRNA lentiviral plasmid | Chan et al., 2015 | N/A |

(*Continued on next page*)

Please cite this article in press as: Singh et al., Disrupting Mitochondrial Copper Distribution Inhibits Leukemic Stem Cell Self-Renewal, Cell Stem Cell (2020), https://doi.org/10.1016/j.stem.2020.04.010



*Continued*

| Reagents or Resource | Source | Identifier |
|---|---|---|
| Software and Algorithms | | |
| GraphPad Prism | Version 5.0 for Mac OS | https://www.graphpad.com/ |
| FlowJo | FlowJo v10.6.1 | https://www.flowjo.com/ |
| Xcalibur v2.1 | Thermo-Fischer Scientific | Part#XCALI-97213 |
| Chromeleon Xpress v7.2 | Thermo-Fischer Scientific | Cat# CHROMELEON7 |
| FastOC v.0.11.2 | Babraham Institute | http://www.bioinformatics.babraham.ac.uk/projects/fastqc/ |
| Trim Galore v.0.4.0 | Babraham Institute | http://www.bioinformatics.babraham.ac.uk/projects/trim_galore/ |
| FastQ-Screen v.0.4.3 | Babraham Institute | http://www.bioinformatics.babraham.ac.uk/projects/fastq_screen/ |
| RSeQC v2.3.7 | | http://rseqc.sourceforge.net/ |
| Tophat v2.0.11 | John Hopkins University | https://ccb.jhu.edu/software/tophat/index.shtml |
| htseq-v.0.6.1p2 | Simon Anders | https://htseq.readthedocs.io/ |
| DESeq v.1.18.0 | Bioconductor | http://bioconductor.org/packages/release/ bioc/html/DESeq.html |
| edgeR, R package, v.3.16.5 | Bioconductor | http://www.bioconductor.org/packages/release/bioc/html/edgeR.html |
| edgeR, R package, v.3.28.21 | Bioconductor | http://bioconductor.org/packages/release/bioc/html/edgeR.html |
| Cytoscape 3.7.1 | The Cytoscape Consortium | https://cytoscape.org/?gclid=CjwKCAjw_tTXBRBsEiwArqXyMp1y9jXNftKoksBpO7Q2BCKzWsvEGPteq7VRCpoVHH22tEsWgCnb7BoCnL4QAvD_BwE |
| Thermo ELEMENT v 3.1.2.242 | Thermo-Fischer Scientific | N/A |
| EnrichmentMap 3.2.1 | The Cytoscape Consortium | https://enrichmentmap.readthedocs.io/en/docs-3.1/ |
| affy, R package, affy_3.0.1 | Bioconductor | https://www.bioconductor.org/packages/release/bioc/html/affy.html |
| sva, R package, sva_3.6.0 | Bioconductor | http://bioconductor.org/packages/release/bioc/html/sva.html |
| ELDA | Hu and Smyth, 2009 | https://www.wehi.edu.au/ |
| Bowtie2 | Langmead & Salzberg, 2012 | http://bowtie-bio.sourceforge.net/bowtie2/index.shtml |
| SAMtools | Li et al., 2009 | http://samtools.sourceforge.net/ |
| Sambamba | Tarasov et al., 2015 | https://lomereiter.github.io/sambamba/ |
| MACS2 | Zhang et al., 2008 | N/A |
| BEDTools | Quinlan, 2014 | https://bedtools.readthedocs.io/en/latest/ |
| EdgeR | Robinson et al., 2010 | https://bioconductor.org/packages/release/bioc/html/edgeR.html |
| Gene set enrichment analysis | Broad Institute | https://www.gsea-msigdb.org/gsea/msigdb/ |
| Other | | |
| LSC+ and LSC- gene set | Ng et al., 2016 | GEO: GSE76009 |
| Bader lab database | This paper | http://baderlab.org/GeneSets |

## RESOURCE AVAILABILITY

### Lead contact

Further information and request for resources and reagents should be directed and will be fulfilled by the Lead Contact, Dr. Aaron D Schimmer (aaron.schimmer@uhn.ca).

### Materials availability

This study did not generate any new unique materials.

Please cite this article in press as: Singh et al., Disrupting Mitochondrial Copper Distribution Inhibits Leukemic Stem Cell Self-Renewal, Cell Stem Cell (2020), https://doi.org/10.1016/j.stem.2020.04.010



### Data and code availability

The following data after ALR inhibition versus control OCI-AML2 cells is available in gene expression omnibus at accession number GEO: GSE146252.

- Expression profiling by high throughput sequencing
- Methylation profiling by high throughput sequencing
- Genome binding/occupancy profiling by high throughput sequencing

## EXPERIMENTAL MODEL AND SUBJECT DETAILS

### Human Cell Lines

OCI-AML2 and NB4 cells were maintained in IMDM (Iscove's modified Dulbecco's medium), supplemented with 10% FBS (fetal bovine serum) (Sigma-Aldrich, Oakville, ON), 100 units/mL penicillin and 100 μg/mL of streptomycin. TEX cells were cultured in IMDM, with 20% FBS, 2 mM L-glutamine, 100 units/mL penicillin and 100 μg/mL of streptomycin, 20 ng/mL stem cell factor (SCF), and 2 ng/mL interleukin-3 (IL-3). TEX cells were generated by immortalizing hematopoietic progenitor cells with TLS-ERG and selecting a population of cells with a leukemic phenotype (Warner et al., 2005). TEX cells exhibit characteristics of AML stem/progenitor cells including the ability to differentiate, arrangement in a hierarchical structure and ability to engraft the bone marrow of immune compromised mice. Jurkat cells were maintained in RPMI 1640 medium, with 10% FBS, 100 units/mL penicillin and 100 μg/mL of streptomycin. 8227 cells were grown in X-VIVO 10 medium (Lonza, 04-380Q) containing 20% BSA, insulin and transferrin along with cocktail of human cytokines IL3 (10ng/ml), SCF (50ng/ml), FLT3 ligand (50ng/ml), G-CSF (10ng/ml), TPO (25ng/ml) and IL-6 (20ng/ml). All cell lines were maintained in a 37°C incubator, supplemented with 5% $CO_2$.

### Animals

Six-twelve week Male or female immunodeficient NOD.Cg-Prkdc$^{scid}$ Il2rg$^{tm1Wjl}$ Tg(CMV-IL3,CSF2,KITLG)1Eav/MloySzJ (NOD-SCID-GF) mice used to transplant TEX cells were obtained from Dr. Connie J. Eaves and bred in our facility (Nicolini et al., 2004). Eight-twelve week old female immunodeficient NOD.CB17-Prkdc$^{scid}$/J (NOD-SCID) and 6-8 week old immunodeficient male Prkdc$^{scid}$ (SCID) mice used for the transplantation of primary AML and OCI-AML2 cells respectively were obtained from the Ontario Cancer Institute.

Mice were randomly assigned to each experimental group. During all experiments, the weights of the mice were approximately 18-30 g with no animals loosing greater than 10% body weight. All animals were housed in microisolator cages with temperature-controlled conditions under a 12-hour light/dark cycle with free access to drinking water, and food. Furthermore, all animal studies were performed in accordance with the Ontario Cancer Institute Animal Use Protocol (AUP): # 1251 (NOD-SCID-GF, NOD-SCID, and SCID).

### Primary AML and Normal Hematopoietic Cells

Primary human AML samples were obtained from peripheral blood or the bone marrow of consenting male or female AML patients, with a malignant cell frequency of 80% among mononuclear cells. Differential density centrifugation was used to isolate AML cells. Peripheral blood stem cells (PBSCs) were obtained from healthy consenting male or female volunteers, donating PBSCs for allogenic stem cell transplantation. PBSCs were isolated by G-CSF stimulation, and leukopheresis. Both primary AML cells, and PBSCs were frozen in 90% FCS +15U/mL of heparin + 10% DMSO. The University Health Network institutional review boards approved the collection and use of human tissue for this study (Research Ethics Board protocol #13-7163). As per regulation, all specimens were de-identified. Each experiment was performed using a single aliquot from a donor. Information about the patients who were the source of the cells is indicated in Table S1.

### Primary AML Cell Cultures for Transduction

After thawing the cells in a 37°C water bath they were washed once in media composed of IMDM 10% FBS, 100 units/mL penicillin, and 100 mg/mL of streptomycin. They were resuspended in X-VIVO 10 supplemented with 20% BIT, 50 ng/ml Flt3-L, 10 ng/mL IL-6, 50 ng/mL SCF, 25 ng/mL TPO, 10 ng/mL IL-3, 10 ng/mL G-CSF at a concentration of $5x10^5$ cells/mL before being transduced.

## METHOD DETAILS

### Plasmids and shRNA knockdown of AML cell lines

Short hairpin RNA (shRNA) in pLKO.1 puromycin-resistant vectors were purchased from Sigma as bacterial stocks. Production of shRNA viruses were done as described previously (Cole et al., 2015). The shRNA targeting ALR (Gene: GFER) coding sequence (Accession number NM_005262), COX17 (Accession number NM_005694), SAHH (Accession number NM_000687) and the control shRNA targeting the GFP sequence (GFP, Accession number clonetechGfp_587s1c1) are mentioned in Table S2.

Lentiviral infections were performed as previously described (Cole et al., 2015). Briefly, 2 mL of virus was added to 5 mL of media containing $5.0 \times 10^6$ cells and protamine sulfate (5 μg/mL) followed by overnight incubation (37°C, 5% $CO_2$). The following day, cells

were centrifuged, washed and re-suspended in 25 mL fresh medium with appropriate puromycin concentration (1.5-2.0 μg/ml) and subjected to selection for 3 days. Equal numbers of live cells in each shRNA treatment were plated for growth assays and counted with trypan blue exclusion staining to measure total viable cells for a period of 11 days. To confirm knockdown at the protein level, 5.0 × $10^6$ cells were collected for immunoblot analysis on day 3 post puromycin selection.

### Plasmids and shRNA knockdown of primary AML cells

For transduction of primary AML cells, COX17 (Accession number NM_005694) and control sequences were first cloned into hairpin-pRS19 vector using the restriction enzyme BsbI. All shRNA, and plasmids were validated by Sanger sequencing before its use in downstream experiments.

Transduction of primary AML cells were performed as described previously (Chan et al., 2015). 24 well plates were coated with Retronectin (20mg/ml in PBS) for 2 hours at room temperature. Further plates were blocked with 2%BSA (W/V) for 30 minutes at room temperature. After removal of BSA 0.5ml of concentrated virus particles in HBBS along with 25mM HEPS was added to each well and plates were centrifuged at 3000 rpm for 5 hours at room temperature to aid in the attachment of viral particles. After centrifugation 0.4ml of viral particle solution was removed and 5x$10^5$ primary AML cells were added to each well in 1ml of X-VIVO 10 medium (20% BIT, 50 ng/ml Flt3-L, 10 ng/mL IL6, 50 ng/mL SCF, 25 ng/mL TPO, 10 ng/mL IL3, 10 ng/mL G-CSF). Plates were centrifuged again at 1300 rpm for 10 minutes and transferred to a 37°C incubator for 24 hours. After 24 hours cells were resuspended in fresh media at a concentration of 1X$10^6$ cells/ml and seeded in 24 well plates at 1ml/well. 5 days later COX17 knockdown was confirmed by qRT-PCR.

### Whole Cell Protein Lysates

For all other immunoblots whole cell lysates were used. To make whole cell lysates, cells (5 3 $10^6$) were washed with PBS followed by cell lysis in RIPA buffer. Protein concentration was measured by Bradford method (Protein assay dye, Bio-Rad, CA, USA).

### Immunoblotting

Cells (5x$10^6$) were washed with PBS followed by cell lysis in RIPA buffer. Protein concentration was measured by Bradford method. Equal amounts of protein were loaded and fractionated on 10%–12% SDS- polyacrylamide gels and transferred to nitrocellulose membranes. Membranes were probed with anti-ALR (Proteintech, 11293-1-AP), COX17 (Proteintech, 11464-1-AP), TIMM9 (Proteintech, 11479-1-AP), TIMM13 (Proteintech, 11973-1-AP), TIMM10 (Proteintech, 11124-2-AP), CCS (Proteintech, 22802-1-AP), TIM23 (BD, 611223), TIM22 (Proteintech, 14929-!-AP), TOM20 (BD, 612278), Drp1 (Millipore ABT155), SAHH (Proteintech, 10757-2-AP), H3-trimethyl K4 (Cell Signaling, 9751), H3-trimethyl k36 (Abcam ab9050), H3-trimethyl k79 (Abcam, ab2621), H3 (Cell signaling, 4499), CHCHD4 (Proteintech, 21090-1-AP) and anti-β-actin (Santa Cruz sc-69879) antibodies.

The antibodies used for immunoblotting can be found in the key resource table.

### Cell viability

For assessment of cell growth and viability MTS (Promega, Cat: G1111, Madison, WI) and Cell-Titer fluor (Promega, Cat: G6082, Madison, WI) were used as per the manufacturer's instructions. Propidium iodide (BD, Cat:556547) was used to measure the cell viability by flow cytometry.

### Colony Formation Assay

To assess clonogenic growth primary cells (1x$10^5$ cells/ml) were plated at equal volumes in duplicate 35 mm dishes (Nunclon, Rochester, USA) to a final volume of 1 mL/dish in MethoCult H4434 medium (StemCell Technologies, Vancouver, BC) and incubated at 37°C, 5% $CO_2$ with 95% humidity. The number of colonies containing 10 or more cells was counted on an inverted microscope for AML samples and for normal progenitors, colonies containing 50 or more cells were counted.

The normal hematopoietic cells used in our clonogenic studies were peripheral blood samples from healthy volunteers who received G-CSF to mobilize their blood stem cells prior to donating peripheral blood for allotransplant.

### Long term culture initiating cell (LTC-IC) assay

AML and normal hematopoietic cells were cultured in IMDM supplemented with 30% FCS at $10^6$/ml with increasing concentrations of MitoBloCK-6 for 48 hours. After this treatment, cells were diluted in Myelocult H5100 plus growth factors, hydrocortisone and MitoBloCK-6 to achieve cell concentrations of: 1x$10^6$, 5x$10^5$, 2.5x$10^5$ and $10^5$/ml. 100 uL of each cell condition was plated in 6 replicates on a layer of MS-5 cell stroma (Itoh et al., 1989) in 96 well plates. Cultures were kept for 5 weeks with periodic changes of the media. After this period, all cells were trypsinized and cultured in semi-solid medium for the development of hematopoietic colonies. The presence or absence of colonies was scored. The scores were tabulated and analyzed with the ELDA program developed by the Walter and Eliza Hall Bioinformatics group (Hu and Smyth, 2009).

### Flow Cytometry

Flow cytometry analysis was performed on FACSCANTO II (BD BioSciences, Mississauga, ON, Canada) or LSRFortessa X-20 (BD Biosciences) using FACS DIVA software. Data was analyzed post-acquisition with FlowJO Software Version 7.7.1 (Treestar, Ashland, OR). Primary and secondary engraftment of AML was measured by staining for CD45-FITC (BD, Cat:347463), CD19-PE (BD,

Cat:349209), CD33 PE-Cy5 (BD, Cat:551377). For differentiation measurements CD11b (BD, 340937), or CD14 (BD, 340436) were used.

### Metabolic flux analysis

Oxygen consumption rate (OCR), and extracellular acidification rate (ECAR) were measured in OCL-AML2 cells after ALR or Cox17 knock-down or after MitoBLoCK-6 treatment using the Seahorse XF-96 analyzer (Seahorse Bioscience, MA, USA). OCR was measured as a marker of electron transport chain activity. Six days after transduction or 24 hours of MitoBLoCK-6 treatment cells were resuspended in unbuffered medium and seeded at $1X10^5$ cells/well in Cell-Tak coated (0.15 mg/well) XF96 plates. Cells were equilibrated in the unbuffered alpha-MEM medium (supplemented with 2% FCS) for 45 minutes at 37°C in a $CO_2$-free incubator before being transferred to the XF96 analyzer. Spare reserve capacity of the mitochondrial respiratory chain was measured by treating cells with oligomycin, and FCCP (carbonyl cyanide p-trifluoromethoxyphenylhydrazone) in succession.

### Respiratory chain complex enzymatic activity

Treated cells were centrifuged, and cell pellets were prepared for assessment of mitochondrial respiratory chain complex activity as previously described (Skrtić et al., 2011). Complex II activity was measured by monitoring malonate-sensitive reduction of 2,6-dichloroindophenol when coupled to complex II-catalyzed reduction of decylubiquinol. Complex IV activity was measured by KCN-sensitive oxidation of ferrocytochrome *c*. Ferrocytochrome *c* was prepared by reducing cytochrome *c* with sodium ascorbate followed by dialysis for 24 hours. The method of citrate synthase activity was based on the chemical coupling of CoASH, released from acetyl-CoA during the enzymatic synthesis of citrate to DTNB (Ellman's reagent, 5,5′-dithiobis(2-nitrobenzoic acid), and the release of the absorbing mercaptide ion was monitored at 412 nm. The enzyme activity was of Complexes II, and IV was normalized to citrate synthase activity.

### Drug combination experiments

The outcome of drug-drug interaction between MitoBlock-6 and daunorubicin or azacytidine was calculated using Excess-over-Bliss additivism (EOBA) model (Borisy et al., 2003). As per this model, EOBA is calculated using this equation:

$$EOBA = C - [A + B - (A \times B)]$$

A corresponds to the fractional inhibition caused by a specific concentration of drug A, B corresponds to the fractional inhibition caused by a specific concentration of drug B, and C corresponds to the fractional inhibition caused by the combination of A and B at these concentrations. Fractional inhibition was calculated as follows:

$$Fractional\ inhibition = 1 - viability(expressed\ as\ a\ fraction\ of\ 1)$$

Positive EOBA scores represent synergistic combinations, negative EOBA scores represent antagonistic combinations, and EOBA scores of zero represent additive combinations. The higher the value of the score (irrespective of the sign), the higher the extent of synergism or antagonism.

### Electron microscopy

The mitochondrial morphology of cells transduced with shRNA in lentiviral vectors targeting ALR, Cox17 or control sequences and post MITOBLOCK-6 treatment, was assessed by transmission electron microscopy (TEM). To perform TEM, cells were harvested at day 8 post-transduction or 48 hr post MITOBLOCK-6 treatment and fixed with a modified Graham-Karnovsky's fixative-4% paraformaldehyde plus 1% glutaraldehyde in 0.1 M phosphate buffer pH 7.2 (PB)-for 30 minutes at room temperature, and 4C overnight. Cells were then washed with phosphate buffer (PB, NaH2P04. H2O+Na2H2PO4) 3 times for 15 minutes. Next, cells were post-fixed with 1% osmium tetroxide buffered with PB for 1 hour and washed again using PB twice for 20 minutes, dehydrated with an ethanol series then infiltrated with propylene oxide. The samples were then resin embedded with Epon, which was polymerized at 40C for 48 hours. Solid epoxy blocks were sectioned on a Reichert Ultracut E microtome to 90 nm thickness, collected on 300 mesh copper grids and counterstained with uranyl acetate and lead citrate. A Hitachi H7000 (Hitachi, Tokyo, Japan) transmission electron microscope with a beam current of 25 mm, was used to view the sections at 60000 X magnification.

### Confocal microscopy

OCI-AML2 cells were cytospun on to glass slides after MitoBloCK-6 treatment. Cells were fixed with 4% paraformaldehyde and permeabilized with 3% BSA in PBS with 0.1% Triton X-100. Further cells were stained with primary (Cox17- Proteintech,11464-1-AP, TOM-20- BD,612278) and fluorochrome conjugated secondary antibody for one hour and forty minutes respectively. Nucleus was stained with DAPI (5μG/ml). Images were taken on SP8 confocal microscope from Leica using a 60X oil lens.

### Copper measurement (ICP-MS)

Copper measurements were performed at Victoria Hospital, London, Ontario, Canada as a paid service. Mitochondria isolated from 10 million cells were resuspended in 500μl milli-que water. 300μl of suspension was made up to 10ml by 0.1% Nitric acid containing the internal standard Rhodium. Standards used were National Institute of Standards and Technology (NIST) traceable standards. Copper was measured on High Resolution Sector Field Inductively Coupled Plasma Mass Spectrometer (ICP-MS (Thermo-Fisher)).

Please cite this article in press as: Singh et al., Disrupting Mitochondrial Copper Distribution Inhibits Leukemic Stem Cell Self-Renewal, Cell Stem Cell (2020), https://doi.org/10.1016/j.stem.2020.04.010



### SAM ELISA

S-adenosylmethionine levels were measured by the SAM Elisa kit from Cell Biolabs (Cat: STA-672) according to the instructions provided with the kit.

### DNA methylation assay

DNA was isolated using the DNeasy Blood and Tissue Kit (QIAGEN). 1μg of DNA was spotted in duplicate onto 0.2 μm nitrocellulose membrane (Amersham) and crosslinked using an FB-UVXL-1000 UV Crosslinker (Fisher) for 20 minutes. Following blocking in 5% milk-TBST for 1 hour at room temperature, membranes were incubated with 5-Hydroxymethylcytoseine antibody (Active Motif, catalog number 39769) and dsDNA (Abcam, ab27156) overnight at 4°. Following 1-hour incubation with secondary antibody (GE Healthcare) proteins were detected by chemiluminescence.

### SAHH activity

S-adenosylhomocysteinase activity was measured by using an SAHH activity kit from Abcam (Cat: ab197002) according to instructions provided.

### Cellular Reactive Oxygen Species

3-4 days after ALR knock-down, cells were stained with Carbocy-H2DCFDA in PBS buffer at 37C for 30 minutes. Afterward cells were resuspended in PBS containing viability dye PI and reactive oxygen species were measured in viable cells. Data was acquired by LSRFortessaX20 (BD Biosciences, FL, USA), and MFI of Carbocy-H2DCFDA in PI negative cells were analyzed using FloJo (TreeStar, OR, USA).

### Seahorse

Oxygen consumption rate (OCR), and extracellular acidification rate (ECAR) were measured in OCI-AML2 cells after COX17 or ALR knock-down or after MitoBloCK-6 treatment using the Seahorse XF-96 analyzer (Seahorse Bioscience, MA, USA). Five days after transduction or 24 hours after MitoBloCK-6 treatment, cells were resuspended in unbuffered medium and seeded at $1x10^5$ cells/well in Cell-Tak coated (0.15 mg/well) XF96 plates. Cells were equilibrated in the unbuffered alpha-MEM medium (supplemented with 2% FCS) or XF Assay medium (supplemented with 4.5 g/l (25mM) glucose + 1mM pyruvate) for 45 minutes at 37C in a $CO_2$-free incubator before being transferred to the XF96 analyzer. Spare reserve capacity of the mitochondrial respiratory chain was measured by treating cells with oligomycin, and FCCP (carbonyl cyanide p-trifluoromethoxyphenylhydrazone) in succession.

### LSC+/LSC- Signature Analysis of MIA40/ALR substrates

Illumina beadchip transcriptomics data containing LSC+ and LSC- sorted AML fractions were obtained from the Gene Expression Omnibus data portal (GSE76008) (Ng et al., 2016) and differential expression between LSC+ and LSC- fractions was calculated using a moderated t test available in the limma R package 3.28.21 incorporating array batch effects in the linear model. A score that ranks genes from top upregulated in the LSC+ fractions to top downregulated when compared to LSC- fractions was calculated using the formula '-log10(pvalue) * sign(logFC)' . The top upregulated 100 genes were used as the LSC+ specific gene list and the top downregulated 100 genes were used as the LSC- gene list.

### Bloodspot database

The expression of GFER (ALR) and COX17 in different hematopoietic progenitors was taken and depicted from Bloodspot database using Normal Human Hematopoiesis (DMAP) dataset.

### ATAC Sequencing

ATAC-seq on control or MitoBLoCK-6 (48 hours, 7.5 μM) treated OCL-AML2 cells was performed as described previously (Corces et al., 2017). ATAC samples were preprocessed according to the ENCODE ATAC-seq pipeline. Single-end reads were aligned to the hg19 genome using Bowtie2 (Langmead & Salzberg, 2012) with the–local parameter, reads with MAPQ scores < 30 were filtered out with Samtools (Li et al., 2009), duplicates were removed using Sambamba (Tarasov et al., 2015), and TN5 tagAlign shifted files were created. MACS2 (Zhang et al., 2008) was used to call peaks with the following parameters: -p 0.01–shift −75–extsize 150–nomodel -B–SPMR –keep-dup all–call-summits. Peaks were later filtered at a q-value threshold of 0.0001 for further analyses.

Peak counts and sizes for each replicate were calculated using a custom Python script, and Jaccard indices for similarities between called peaks was calculated using BEDTools (Quinlan, 2014).

Differentially accessible regions were calculated using the DiffBind and EdgeR (Robinson et al., 2010) packages in R. Regions with an absolute fold-change > = 1.5 and an FDR value ≤ 0.05 were defined as significantly differentially accessible regions.

### Classification of ATAC gene lists as HSC/stem or myeloid/granulocytes

Changes in gene expression between LSC+ and LSC- fractions were mapped to the Gene Expression Omnibus dataset GSE24759 (DMAP) (Novershtern et al., 2011), containing Affymetrix GeneChip HT-HG_U133A Early Access Array gene expression data of 20 distinct hematopoietic cell states. GSE24759 data were background corrected using Robust Multi-Array Average (RMA), quantile normalized using the expresso function of the affy Bioconductor package (affy_1.38.1, R 3.0.1), array batch corrected using

Please cite this article in press as: Singh et al., Disrupting Mitochondrial Copper Distribution Inhibits Leukemic Stem Cell Self-Renewal, Cell Stem Cell (2020), https://doi.org/10.1016/j.stem.2020.04.010



the ComBat function of the sva package (sva_3.6.0). Gene differential expression was calculated between HSC and granulocyte population using limma t test. A scatterplot is showing on the x axis the LSC+/LSC- expression score (-log10 pvalue) and the t-value of the HSC/granulocyte expression score.

### RNA sequencing analysis

Prior to analysis, read adapters and low quality ends were removed using Trim Galore v. 0.4.0. Reads were aligned against hg19 using Tophat v. 2.0.11. Read counts per gene were obtained through htseq-count v.0.6.1p2 in the mode ''intersection_nonempty.''

Gene read counts were normalized using the TMM method available from the edgeR_3.24.3 package. After removing genes whose cpm (counts per million reads) were less than 0.5 to remove noise, edgeR was used to estimate differential expression by applying a generalized linear model between the control samples and the cells isolated after MB6 treatment and MB6 and PEN treatment. A score that ranks genes from most upregulated in the MB6 samples and MB6PEN samples to most downregulated when compared to control samples was calculated using the formula '-log10(pvalue) * sign(logFC)'.

### Pathway and network analysis

Gene set enrichment analysis (GSEA software, https://www.gsea-msigdb.org/gsea/msigdb/) was used to compare samples using the MB-6 and MB-6/PEN ranked lists of genes and the Bader lab gene-set file (http://baderlab.org/GeneSets) as the pathway database. GSEA was run using default parameters. GSEA results were visualized as a network using Cytocape 3.7.1 and EnrichmentMap 3.2.1. AutoAnnotate 1.3.2 automatically labeled pathway modules using most frequent words. LSC+ and LSC- gene lists were added as gene-sets to the enrichment map and the significance of overlap with gene-sets was calculated using the EnrichmentMap post analysis integrated hypergeometric test.

Single sample gene set enrichment analysis (ssgsea) was run using the R package GSVA_1.30.0 using normalized counts per million (CPM). Ssgsea was run against selected pathway modules from the GSEA/EnrichmentMap analysis and against tumor derived HSC, progenitor, GMP and myeloid specific gene lists (van Galen et al., 2019).

Enrichment scores were represented as violin plots and a heatmap created using gplots_3.0.1.2 and ggplot2_3.2.1 function. Pairwise t tests were applied on the enrichment scores obtained for the groups and the p values were corrected for multiple hypothesis testing.

### ATACseq gene list and chromosomal position

To examine concomitant open gene regions, genes that were retrieved from the ATAC seq data were plotted on a chromosome map using the chromoMap R package. In addition, Enrichr was used with the Chromosome Location hg19 database to assess chromosome position enrichment in this gene list (Chen et al., 2013; Kuleshov et al., 2016).

### Targeted DNA Methylation

Methyl-seq profiling is performed on 9 samples and libraries were constructed as described previously (Kacmarczyk et al., 2018) (TruSeq-Methyl Capture EPIC, cat # FC-151-1002, Illumina Inc., San Diego, CA). Briefly, following company's protocol libraries were prepared using 500 ng of genomic DNA. DNA was sonicated using a Covaris LE220 sonicator (Covaris, Woburn, MA) to obtain products of 180–220 bp. DNA was end-repaired, A-tailed and ligated with methylated indexed-adapters to create pre-capture DNA libraries. All pre-capture libraries were hybridized to the EPIC oligos. Hybridized products were subjected to bisulfite conversion. The bisulfite-treated libraries were PCR-amplified. Libraries were sequenced 100 bp paired-end on Illumina NovaSeq-6000. Preprocessing including adaptor trimming using cutadapt and quality control using FastQC were performed. Quality-trimmed paired-end reads were aligned to the reference genome (hg38) using Bismark (Krueger & Andrews, 2011) and Bowtie2 (Langmead & Salzberg, 2012) using default parameters.

Data is analyzed using the MethylKit R package. Differentially methylated sites were identified and ranked based on percentage of methylation difference > 25% and q-value < 0.01. Differentially methylated sites were mapped and associated to their nearby genes (5kb upstream, 1kb downstream of transcription start site) for annotation purpose. Gene Ontology (GO) and pathway analysis were performed using default parameters of Bioconductor package rGREAT (McLean et al., 2010).

### Animal Studies

TEX cells (1-2X10$^6$) or primary AML cells (1x10$^5$) were transduced with ALR, COX17 or control sequences were injected in the right femur of sub-lethally (2 grays) irradiated NOD-SCID-GF mice (Nicolini et al., 2004). 5-6 weeks after injection mice was sacrificed and engraftment of human cells was measured in the left femur. For TEX cells human CD45 positive cells were quantified by flowcytometry. For primary AML cells GFP-CD45 positive cells were quantified. Engraftment potential was calculated as described below. Mice were observed routinely for health assessment and survival.

To assess the impact of ALR inhibition *in-vivo* OCI-AML2 cells transduced with ALR, or control sequences were injected in the back flaps of male SCID mice, tumor volume and mice survival was measured over time.

To measure the role of ALR inhibition by MitoBloCK-6, OCI-AML2 cells (1x10$^6$) were injected in the back flaps of male SCID mice and animals were treated with MitoBloCK-6 (80 mg/kg, i.p. 5 of 7 days/twice daily, 16 doses) or vehicle control. Tumor volume was measured every 2-3 days. mice body weight was measured along the course of the experiment. At the end of experiment mice were

sacrificed, peripheral blood was collected and alkaline phosphatase (ALP), aspartate transaminase (AST), bilirubin (Bili), creatine kinase (CK), creatinine (Cr) levels were measured by Idexx Laboratories (Ontario, Canada).

Primary AML cells were injected in the right femur of sub-lethally irradiated (2 grays) NOD-SCID mice were conditioned with 200 mg of anti-mouse CD122 48 hours before transplantation. 10 days after injection, mice were treated with vehicle or MitoBloCK-6 (80mg/kg i.p.; twice daily 10 days, 20 doses). 6-8 weeks after transplantation engraftment was measured in left femur by measuring the percentage of CD45-CD33 positive and CD19 negative cells by flow cytometry.

### Calculation of Engraftment Potential

Engraftment potential was measured as described previously (Pei et al., 2018). Prior to injection, the transduction efficiency was measured by calculating % of GFP positive cells via flow cytometry. After sacrificing the mice the % of GFP and CD45 positive cells was measured and relative engraftment was calculated by the formula published earlier.

## QUANTIFICATION AND STATISTICAL ANALYSIS

Prism Graph Pad 6.0 was used to perform statistical analysis and data plotting. Data is represented as mean ± standard deviation (SD). An unpaired Student's t test was used to calculate significance between two groups. Logrank test was used to measure significance in Kaplan-meier plots for survival curves. P value for LTC-IC assay was calculated from Chi-square score and degree of freedom (DF). The level of significance is represented as follows: *$p < 0.05$, ** $p < 0.01$, *** $p < 0.001$, **** $p < 0.0001$.